Major zircon megacryst suites of the Indo-Pacific lithospheric margin (ZIP) and their petrogenetic and regional implications

Lin Sutherland, Ian Graham, Gregory Yaxley, Richard Armstrong, Gaston Giuliani, Paul Hoskin, Victor Nechaev & Jon Woodhead

Mineralogy and Petrology

ISSN 0930-0708

Miner Petrol
DOI 10.1007/s00710-015-0421-3

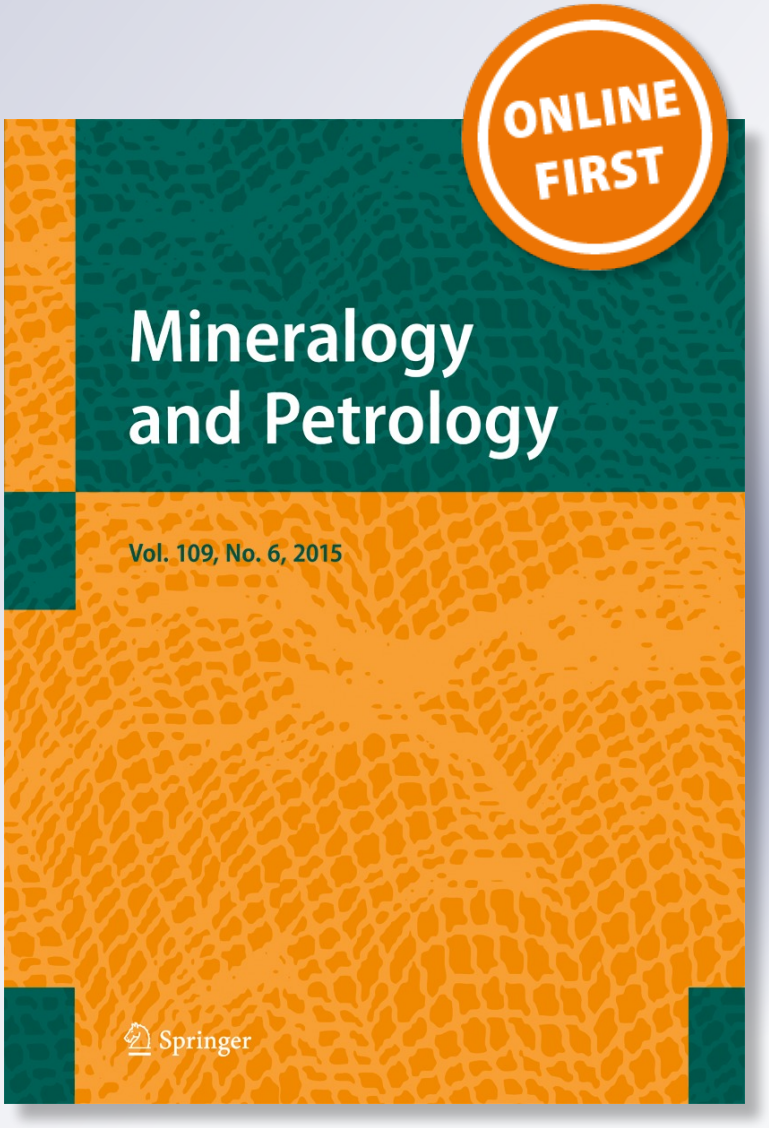

Springer

Miner Petrol
DOI 10.1007/s00710-015-0421-3

ORIGINAL PAPER

Major zircon megacryst suites of the Indo-Pacific lithospheric margin (ZIP) and their petrogenetic and regional implications

Lin Sutherland[1,2] · **Ian Graham**[1,3] · **Gregory Yaxley**[4] · **Richard Armstrong**[4] · **Gaston Giuliani**[5] · **Paul Hoskin**[8] · **Victor Nechaev**[6,7] · **Jon Woodhead**[9]

Received: 29 May 2015 / Accepted: 16 December 2015

Abstract Zircon megacrysts (± gem corundum) appear in basalt fields of Indo-Pacific origin over a 12,000 km zone (ZIP) along West Pacific continental margins. Age-dating, trace element, oxygen and hafnium isotope studies on representative zircons (East Australia–Asia) indicate diverse magmatic sources. The U–Pb (249 to 1 Ma) and zircon fission track (ZFT) ages (65 to 1 Ma) suggest thermal annealing during later basalt transport, with < 1 to 203 Ma gaps between the U–Pb and ZFT ages. Magmatic growth zonation and Zr/Hf ratios (0.01–0.02) suggest alkaline magmatic sources, while Ti—in—zircon thermometry suggests that most zircons crystallized within ranges between 550 and 830 °C. Chondrite-normalised multi-element plots show variable enrichment patterns, mostly without marked Eu depletion, indicating little plagioclase fractionation in source melts. Key elements and ratios matched against zircons from magmatic rocks suggest a range of ultramafic to felsic source melts. Zircon O-isotope ratios ($\delta^{18}O$ in the range 4 to 11‰) and initial Hf isotope ratios (εHf in the range +2 to +14) encompass ranges for both mantle and crustal melts. Calculated Depleted Mantle (TDM 0.03–0.56 Ga) and Crustal Residence (0.20–1.02 Ga) model ages suggest several mantle events, continental break-ups (Rodinia and Gondwana) and convergent margin collisions left imprints in the zircon source melts. East Australian ZIP sites reflect prolonged intraplate magmatism (~85 Ma), often during times of fast-migrating lithosphere. In contrast, East Asian-Russian ZIP sites reflect later basaltic magmatism (<40 Ma), often linked to episodes of back-arc rifting and spreading, slow-migrating lithosphere and slab subduction.

Editorial handling: NV Chalapathi Rao

Electronic supplementary material The online version of this article (doi:10.1007/s00710-015-0421-3) contains supplementary material, which is available to authorized users.

✉ Ian Graham
i.graham@unsw.edu.au

[1] Geoscience, Australian Museum, 6 College Street, Sydney, NSW 2010, Australia

[2] School of Science and Health, Western Sydney University, Locked Bag 1797, Penrith South DC, NSW 1797, Australia

[3] School of Biological, Earth and Environmental Sciences, University of New South Wales, Sydney, NSW 2052, Australia

[4] Research School of Earth Sciences, Australian National University, Canberra, ACT 0200, Australia

[5] Université de Lorraine, CRPG UMR 7358 CNRS-UL, BP20, 54501 Vandoeuvre-lès-Nancy, France

[6] Far East Geological Institute, 159, PR. 100-LET, Vladivostok 690022, Russia

[7] Engineering School, Far Eastern Federal University, 8 Sukanova Str, Vladivostok 690950, Russia

[8] Department of Geology, University of Namibia, Private Bag 13301, Windhoek, Namibia

[9] School of Earth Sciences, University of Melbourne, Parkville, VIC 3010, Australia

Published online: 09 January 2016

Introduction

Large gem-quality zircons commonly accompany sapphire ± ruby in many placer and volcanoclastic deposits that were derived from alkali basalt volcanic fields (Gübelin 1982; Groat 2014). Crystals range in size up from macrocrysts (0.5–1 cm) into megacrysts (>1 cm) and represent xenocrysts entrained in basaltic magmas during their ascent, before erosional dispersal and concentration in placers (Tietz and Büchner 2007; Seifert et al. 2008, 2012; Abduriyim et al. 2012). The gem corundum receives preferential study because of its greater commercial value (Shor and Weldon 2009), while the zircon provides considerable geochronologic and geochemical data related to its genesis, as does zircon included in corundum (Guo et al. 1996a, b; Sutherland et al. 2002a, b, 2015; Siebel et al. 2009; Izokh et al. 2010; Seifert et al. 2012). In some deposits zircon megacrysts predominate over corundum and even become the mining target, as in the Ratanakiri deposits, Cambodia, where zircon yields effective heat-treatment color changes (Smith and Balmer 2009; Wittwer et al. 2013). Only rare zircon ± corundum-bearing xenoliths or outcrops indicate likely source rocks (Coenraads et al. 1995; Pisutha-Arnond et al. 1998; Upton et al. 1999; Monchoux et al. 2006; Schmitt 2006; Giuliani et al. 2009; Paquette and Mergoil-Daniel 2009). Zircons included in corundum (Sutherland et al. 2015) form a geochemical subset within the larger zircon megacryst story and are not dealt with in detail in this study.

Zircon megacryst suites represent magmatic and some metamorphic processes (Hinton and Upton 1991; Sutherland and Fanning 2001; Garnier et al. 2005; Izokh et al. 2010; Khamloet et al. 2014) and include 'kimberlitic' type zircons (Corfu et al. 2003; Simonetti and Neal 2010). They represent a diverse range of crystallizations, when matched against zircon classification and regression trees (CART; Belousova et al. 2002). Distinction of magmatic zircons relies on crystal morphology, oscillatory zoning and otherwise non-recrystallized textures, rare earth element (REE) data or preserved high Th/U ratios (e.g. zircon groups in a North China granulitic xenolith suite, Liu et al. 2004). Igneous zircons commonly have Th/U > 0.5 (Hoskin and Schaltegger 2003; Zheng et al. 2005b), although ratios depend on co-crystallising phases and can develop values < 0.5 (Kirkland et al. 2014). Zircons formed in magmas where feldspar, particularly plagioclase, crystallized tend to develop negative Eu anomalies (Hinton and Upton 1991), while those grown in plagioclase-poor systems or at pressures above plagioclase stability lack noticeable Eu depletion (Sutherland 1996; Siebel et al. 2009).

Precise dating of zircon utilises several U-Th-Pb isotopic methods (Hanchar and Hoskin 2003). Methods employed in previous studies on zircon megacrysts from western Pacific margin basalt fields include isotope dilution-thermal ionisation mass spectrometry (ID-TIMS), secondary ion mass-spectrometry (SIMS), including sensitive high resolution ion microprobe (SHRIMP) methods, laser ablation-inductively coupled plasma-mass spectrometry (LA-ICP-MS) and fission track (FT) techniques (Graham et al. 2008). Very young zircons (<1 Ma) can be dated using high-spatial-resolution (^{230}Th/ ^{238}U) disequilibrium dating, SHRIMP, or multi-collector LA-MC-ICP-MS analysis. The Th/U ratios of the hosts, however, need to be known or estimated, to allow accurate U–Th disequilibrium calculations (Schmitt 2006; Cocherie et al. 2009). This is an important limiting factor for very young megacryst zircons divorced from their sources (Sutherland et al. 2014, 2015), as in this study.

Zircon/corundum generation in the lithosphere is complex and studies involve mineral, melt and fluid inclusions, oxygen isotope ratios and chronologic investigations (Upton et al. 1999, 2009; Limtrakun et al. 2001; Yui et al. 2003, 2006; Giuliani et al. 2005; Garnier et al. 2005; Graham et al. 2008). A few analogues for zircon/ corundum megacryst sources include a monzonite dyke in Late Precambrian gneisses in Kenya (Simonet et al. 2004), nepheline-bearing gneisses in Malawi (Ashwal et al. 2007), Cretaceous albititic dykes in uplifted mantle peridotites in the French Pyrenees (Monchoux et al. 2006; Pin et al. 2006) and syenitic xenoliths in Paleogene-Neogene volcanic centres, Massif Central, France (Giuliani et al. 2009; Paquette and Mergoil-Daniel 2009).

The zircon ± corundum/basalt megacryst association reaches its greatest regional expression within the intraplate basaltic belts along the western Pacific continental margins in eastern Australasia, Asia and Russia (Vysotskii et al. 2002, 2015; Graham et al. 2008; Sutherland and Meffre 2009; Nechaev et al. 2009; Izokh et al. 2010; Yu et al. 2010; Abduriyim et al. 2012; Khamloet et al. 2014). This 12,000 km long zircon megacryst Indo-Pacific zone (Fig. 1) has no comparable counterpart elsewhere and is given the acronym ZIP. Some ZIP host basalts involve deeper mantle generations of alkaline basaltic magmas and can intersect a range of pre-existing gem-bearing sialic igneous and metamorphic bodies (He et al. 2011; Khamloet et al. 2014).

To further study these zircon megacryst suites, new detailed textural, geochronological and geochemical data are given from six representative ZIP sites (between 42° S and 45° N; East Australia, South-East Asia, East Russia). The data will augment previous scattered studies on other ZIP sites (Figs. 1, 2 and 3). This study aims to:

1. Define the ZIP zone in terms of its zircon characteristics, geological settings and tectonic events.
2. Describe internal textures of zircons to illustrate their growth characteristics.
3. Utilise a range of age-dating, trace element and isotopic analytical techniques to define the crystallization and

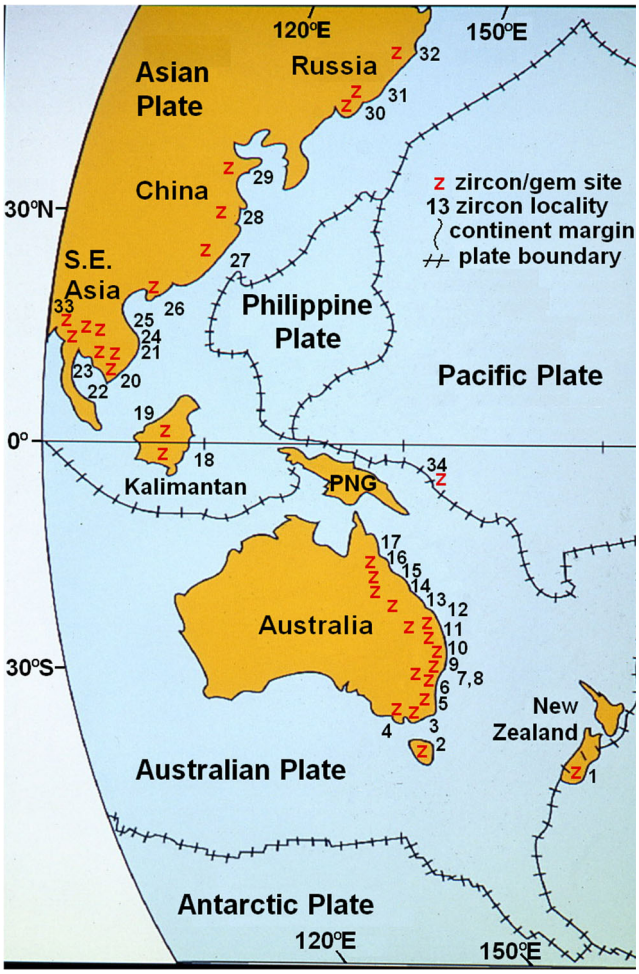

Fig. 1 Map showing the distribution of zircon megacryst locations (the 'ZirconZip'), West Pacific continental margins (1 = Otago, New Zealand; 2 = Weldborough, NE Tasmania; 3 = eastern Victoria; 4 = central-west Victoria; 5 = Tumbarumba, NSW; 6 = Oberon, NSW; 7 = Wellington, NSW; 8 = western Blue Mountains, NSW; 9 = Barrington Tops, NSW; 10 = Yarrowitch, NSW; 11 = Main Range, QLD; 12 = Bunya Mountains, QLD; 13 = Anakie, QLD; 14 = Nebo Province, QLD; 15 = Chudleigh, QLD; 16 = McBride Province, QLD; 17 = McLean Province, QLD; 18 = SE Kalimantan; 19 = Central Kalimantan; 20 = South Vietnam; 21 = Cambodia; 22 = Chanthanburi-Trat region, Thailand; 23 = Bo Ploi region, Thailand; 24 = Denchai, Thailand; 25 = Laos; 26 = Hainan Island, China; 27 = Changle, China; 28 = eastern China; 29 = northern China; 30 = southern Primorye, Russia; 31 = northern Primorye, Russia; 32 = Sovgavan Plateau, Russia; 33 = Myanmar; 34 = Malaita, Solomon Islands)

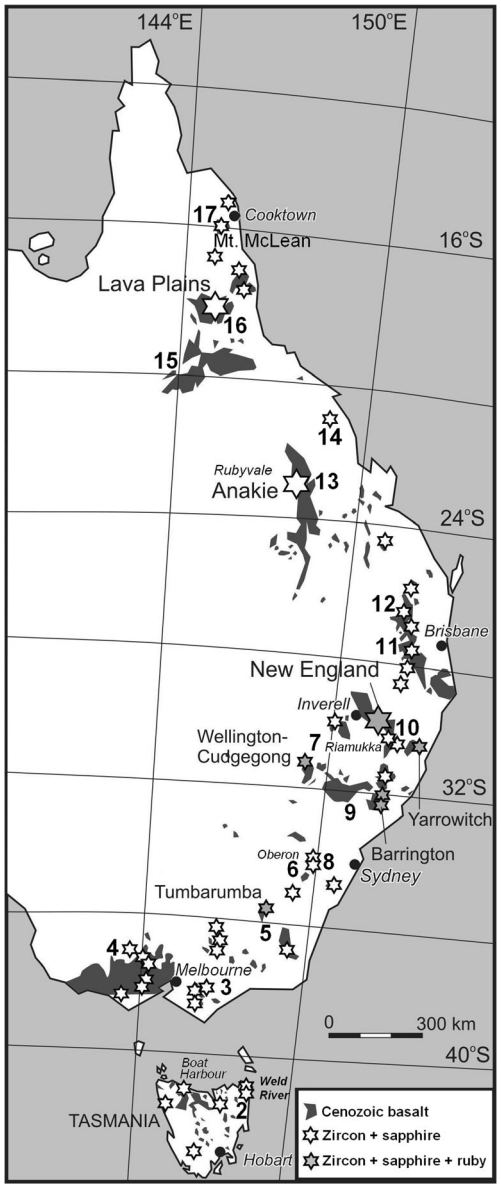

Fig. 2 Map of eastern Australia showing distribution of main zircon megacryst locations in relation to the intraplate Cenozoic basalt fields of eastern Australia. Adapted from Graham et al. (2008)

resetting ages, chemical affinities and isotopic variations within the zircons.

4. Appraise the zircon geochemistry in relation to potential source rocks.
5. Integrate and co-ordinate new and previous zircon megacryst data to model ZIP genesis.
6. Consider the implications of the ZIP model in terms of its lithospheric and geodynamic contexts.
7. Outline further studies needed to test proposed Zircon Zip models.

Geological setting

The ZIP intraplate basalts were erupted through late Precambrian to early Cenozoic rifted blocks, fold belt terranes and less-deformed late Paleozoic to Cenozoic sedimentary cover (Scheibner 1999; Khanchuk 2001; Yu et al. 2010; Barr and Cooper 2013). The underlying terranes trend roughly north–south in eastern Australia (Veevers 2001) and in SE Asia they flank the Indochina cratonic block and converge in a trend northwards (Hoang and Flower 1998; Metcalfe 1999). The intervening region is largely disrupted by the Melanesian-Indonesian arc and strike-slip systems (Hall and Spakman 2003). In eastern China, deep-faulted tectonic

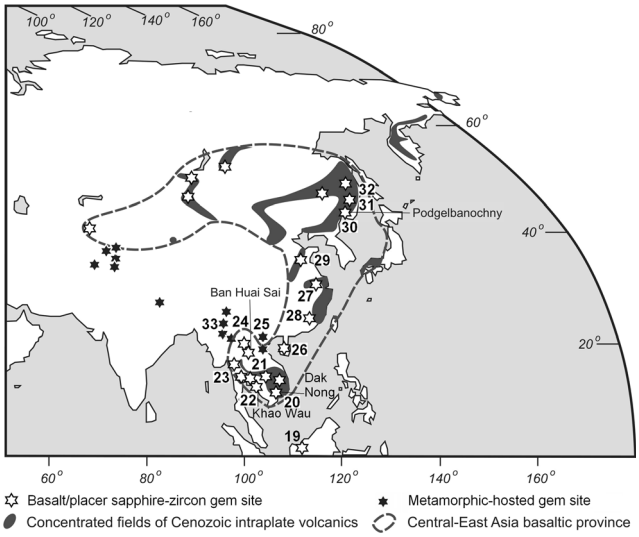

Fig. 3 Map of central, eastern and SE Asia showing distribution of main zircon megacryst locations in relation to intraplate Cenozoic basalt fields, with zircon-corundum placer deposits (*open stars*) and hard rock-hosted corundum-zircon deposits (*closed stars*). Adapted and modified from Graham et al. (2008)

blocks partly control the basaltic emplacements and zircon megacryst characteristics (Zou et al. 2000; Qiu et al. 2005, 2007). In north-eastern Asia, the Mesozoic-Cenozoic fold belt and fault systems are largely north-easterly/south-westerly in strike and include rift-related basalt fields (Okamura et al. 2005).

The ZIP sites are flanked to the east by extinct marginal spreading basins and subsidiary offset rifts that formed behind the western Pacific island arc-subduction systems (Miller et al. 2006). These include the Late Cretaceous-Early Cenozoic Tasman-Coral Sea spreading basins (Gaina et al. 1998; Crawford et al. 2003; Sutherland et al. 2012) and the Neogene South China Sea and Japan Sea spreading basins (Itoh et al. 2006; Sun et al. 2009). These basins involved thermal rifting (e.g. the 100 to 60 Ma Tasman-Cato-Coral Sea margins; Moore et al. 1986; Marshallsea et al. 2000). Such rifts could provide a quasi-continuous source of sub-lithospheric melting that promoted zircon and corundum crystallising events among prolonged basaltic pulses (Sutherland 1996; Sutherland and Fanning 2001; Sutherland 2003).

In eastern Australia, the ZIP zone follows the north–south Indian-Pacific asthenospheric mantle boundary, which is reflected in the basalt field MORB-type isotopic signatures (Zhang et al. 1999; Sutherland 2003). In the southmost section, ZIP basalt fields include HIMU OIB-type isotopic signatures (Khin Zaw et al. 2006; Sutherland and Meffre 2009). The eastern Asian ZIP margin includes rift-related basalts with both lithospheric and asthenospheric geochemical signatures and isotopic changes have been attributed to different underlying domains and their interactions (Mukasa et al. 1996; Hoang and Flower 1998; Zou et al. 2000; Okamura et al. 2005; Zheng et al. 2005a). The basalts generally exhibit Gondwanan Indian Ocean mantle signatures, without much evidence of Pacific mantle input.

The ZIP basalts lie within dynamic tectonic settings along the western Pacific margin in which plate motions are carrying continental and former sea-floor lithosphere over zones of hot upwelling asthenosphere (Electron Appendix 1). Along the northern Asia-Russia margin, this setting includes intervening colder regions under extinct late Cenozoic spreading floors and areas where slabs are descending from proximal active subduction along the Japanese arc.

Zircon sampling sites

The studied zircon sites (Table 1) are described in terms of local geology and literature in Electronic Appendix 2 and are only outlined here.

Eastern Australia

The study sites (Fig. 2) include the southern Weldborough field (147.9° E, 41.2° S), NE Tasmania, ~ 140 km west of the Tasman Sea spreading floor, the central Yarrowitch (152.0° E, 31.3° S) and Riamukka, New South Wales fields, ~ 150 to 180 km west of the Tasman floor and the northern Mount McLean field (144.8° E, 15.8° S), NE Queensland, ~ 500 km southwest of the Coral Sea spreading floor. Other zircon megacryst sites provide extensive comparative data on crystal morphology, fission track and U–Pb geochronology, trace element geochemistry and oxygen and hafnium isotope results (Hollis and Sutherland 1985; Sutherland 1996; Worden et al. 1996; Sutherland et al. 1998, 2014, 2015; Sutherland and Fanning 2001; Birch et al. 2007; Abduriyim et al. 2012; Kennedy et al. 2014).

South-East Asia

The study sites (Fig. 3) lie within complex tectonic mineralized basement terranes (Khin Zaw et al. 2014). They include a southern Vietnam and a northern Laos field. The Dak Nong (Gia Nghia), southern Vietnam field (106.8° E, 12.1° N) lies ~ 350 km northwest of the South China Sea spreading floor. The Ban Huai Sai, Laos field (100.2° E, 22.3° N) lies ~ 1800 km northwest of that floor. The basalts range between 0 and 18 Ma in age, include Qz and Ne-normative types and zircon + corundum hosts largely appear in the younger basalts (Hoang and Flower 1998; Sutherland et al. 2002b; Garnier et al. 2005). The basalts mostly ascended along rift structures, bounded by strike-slip faults, within Archaean to Palaeozoic terranes, flanked by Mesozoic sedimentary and volcanic sequences (Lan et al. 2001).

Table 1 Investigated zircon megacrysts, procedures and sample sources

Locality		Description	Procedure	Sample source
East Australia				
WRT Z1	Weldbrough, Weld River, NE Tas	Moderately rounded, polished; equant to prismatic; white, pink, yellow, red brown grains; 3-8 mm	ICP-MS[a] U-Pb[a], F.T.[b,c]	Alluvial sample, Australian Museum collection
YAR Z1	S. Fenwicks Creek, Yarrowitch, NSW	Anhedral; polished, corroded; equant; pale (white, pink, brown, yellow) grains; 2–7 mm	F.T.[a]	Palaeoalluvial bed, AM collection
YAR Z2	As above	Angular to rounded; corroded; amber-yellow grains	F.T.[a]	Alluvial sample, AM collection
YAR Z3	As above	Angular to rounded; well-polished; orange-red grains	F.T.[a]	As above
YAR Z4	As above	Angular to well-rounded; polished; deep-red grains	F.T.[a]	As above
YAR Z5a	As above	Subhedral to euhedral; equant to prismatic; orange-brown grains	ICP-MS[a] U-Pb[a]	As above
YAR Z5b	As above	Small; complex equant; white grains	ICP-MS[a] U-Pb[a]	As above
YAR Z5c	As above	Subhedral; resorbed, highly polished; equant, deep-red grains	ICP-MS[a] U-Pb[a]	As above
YAR Z5d	As above	Subhedral; part-resorbed pink grains	ICP-MS[a] U-Pb[a]	As above
YAR Z6	As above	Subhedral; resorbed; equant; pink, yellow, blue-green, brown-green grains	EMP[a]	As above
YAR Z6	As above	Subhedral; resorbed; equant; pink, yellow, blue-green, brown-green grains	EMP[a]	As above
D53800	As above	Megacrysts, pink, yellow, green	EMP[a] $\delta^{18}O$[a]	As above
D53795	Riamukka, NSW	Zircon-magnetite composite	ICP-MS[a] $\delta^{18}O$[a]	Alluvial sample AM collection
MML Z	NW Mt McLean cone, Qld.	Subhedral to rounded; equant to ovoid; clear, yellow-grey, red-brown grains	F.T.[a]	Eluvial sample, AM collection
MML Z1	As above	Anhedral to rounded; highly polished ovoid; glassy clear grains; 1.5-7 mm	U-Pb[a] ICP-MS[a]	As above
East Asia				
D53796	Khao Wua	Zircon-magnetite-sapphire xenolith	$\delta^{18}O$[a] EMP[d] U-Pb[e]	Alluvial sample AM collection
BHSL Z1	2 km W. Ban Huai Sai town, Laos	Anhedral to subhedral; corroded equant to sub-prismatic; red-brown grains; 3–6 mm.	F.T.[a]	Alluvial sample, AM collection
BHSL Z2	As above	Most euhedral grains from sample BHSL Z1	U-Pb[a] ICP-MS[a]	As above
GNV Z1	Gia Nghia, Dak Nong, Vietnam	Rounded to subhedral; corroded; glassy clear grains; 7–23 (av.15) mm	F.T.[a]	Alluvial sample, AM collection
GNV Z2	As above	Rounded to subhedral; corroded Fe oxide-stained, glassy clear grains	F.T.[a]	As above
GNV Z3	As above	Rounded to subhedral; corroded; glassy brown grains	F.T.[a]	As above
GNV Z4	As above	Euhedral; prismatic; glassy clear grains	U-Pb[a] ICP-MS[a]	As above
East Russia				
PBV Z1[a]	Podgelbanochny Creek Primoré, East Russia	Subhedral; resorbed; equant to sub-prismatic; lustrous orange-brown grains; 0.5–5 mm	F.T.1, U-Pb[a] ICP-MS[a]	Alluvial sample, AM collection
PBV Z1b	As above	Subhedral; pitted; equant to sub-prismatic; lustrous brown grains	As above	As above

Table 1 (continued)

Locality		Description	Procedure	Sample source
PBV Z1c	As above	As above, but pale grains	As above	
PBV Z1d	As above	Anhedral to subhedral; partly resorbed; minute; clear grains	F.T.[a]	

F.T. dating, Geotrack International, Melbourne, Vic; U-Pb dating, SHRIMP facility, LA-ICP-MS Australian National University, Canberra, ACT; EMP analyses, University of Western Sydney, NSW

[a] This paper

[b] Yim et al. (1985)

[c] Khin Zaw et al. (2006)

[d] Coenraads et al. (1995)

[e] Sutherland et al. (1998)

Zircon megacrysts from the adjacent Cambodian and Thailand basalt fields include low-U types (between U 30 and 80 ppm) that give close knit U–Pb formation ages from 1 to 11 Ma, always slightly older than their basalt hosts (Davis and Barr 1995). The very low Th/U ratios of these zircons were attributed by those authors to fluids generated from a subducted slab.

Far eastern Russia

Zircons and sapphire megacrysts derived from Late Cenozoic (16 to 3 Ma) basalt fields appear in placers in the Primore region (Vysotskii et al. 2002; Khanchuk et al. 2003; Chashchin et al. 2007; Graham et al. 2008). The zircons studied here (Fig. 3) came from the 11 to13 Ma Podgelbanochny alkali basalt field (133.1° E, 43.3° N). Earlier crystal studies and a U–Pb (SHRIMP) age (11.2 Ma) by Akinin et al. (2004) and preliminary ZFT and O isotope results suggest a mantle origin for the gem association (Nechaev et al. 2009). These results are expanded here with further detailed FT and U-Pb dating and geochemistry on Pogelbanochny zircons.

Analytical methods

Zircon grains were picked out from heavy mineral concentrates panned during field sampling at individual localities or from well-documented material already present in the Australian Museum collections (Table 1). Zircon from concentrates from Yarrowitch and Podgelbanochny were studied for surface features by scanning electron microscopy (SEM) photography using a LEO 435 VP SEM with Robinson backscattered electron detector and Everhart-Thomley SE secondary detector, at the Australian Museum (Fig. 4). Samples were first reduced to < 20 mm and gold sputter coated. Accelerating voltage was 29 kV and working distance was 25 mm. Polished zircons from all localities (Table 1) were then documented prior to analysis by reflected and transmitted light photomicroscopy and cathodoluminescence (CL) and back scattered electron (BSE) imaging on a Hitachi S-2250 N (SEM), Research School of Earth Sciences, Australian National University, Canberra (Electronic Appendix 3). Zircons were then embedded in mounts and polished, for analytical runs together with appropriate standards.

Geochronology

Zircon grains from each site were dated by fission track and U-Pb isotope methods (Electronic Appendix 4). The zircon

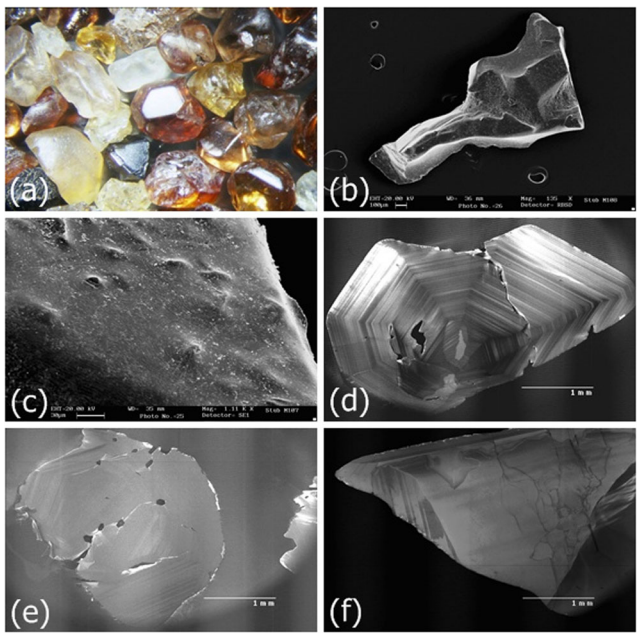

Fig. 4 Zircon megacryst morphology and growth features. **a** typical zircon megacrysts, up to 5 mm in size, Yarrowitch, NSW **b** SEM image of corroded zircon with scour features, due to magma transport, Podgelbanochny, Primorye **c** SEM image of Podgelbanochny zircon megacryst with surface 'pimpling' **d** CL image of zircon megacryst, Yarrowitch, NSW with oscillatory growth zonation **e** CL image of zircon megacryst, Ban Huai Sai with euhedral negative inclusions and oscillatory growth zonation **f** CL image of zircon megacryst, Weld River (older grain) with decompression fractures and micro-breccia zone

FT results (Table 2) represent post-formation heating events for these basalt-transported xenocrysts, as tracks become partially annealed above 200–230 °C and usually annealed completely above 750–900 °C (Yamada et al. 1995). The U-Pb isotope results (Table 3), in comparison, are little affected by potential Pb loss from diffusion between 900 and 1500 °C and largely represent formation or re-crystallization ages, on the basis of experiments using common Pb^{2+} (Cherniak and Watson 2001). However, radiogenic lead which produces smaller Pb^{4+} or Pb^{6+}ions may promote faster diffusion and lower closure temperatures. The smaller Pb^{4+} ion, however, is more compatible with Zr, and diffusion is insignificant unless zircons became annealed at < 600–650 °C (Mezger and Krongstad 2004). The age-dating procedures are described in Electronic Appendix 4.

Geochemistry

Zircons from Yarrowitch were analysed for their main elements by electron microprobe (EMPA), while zircons from all sites were analysed for trace elements by LA-ICP-MS. Hafnium and lutetium isotopic compositions (Woodhead et al. 2004) were analysed on most of the same grains that provided the U–Pb ages. The O isotope determinations ($\delta^{18}O$) were made on selected zircon megacrysts and zircon composites using facilities and ion microprobe techniques described in Giuliani et al. (2000). Details of the analytical procedures are described in Electronic Appendix 4.

Results

Zircon morphology and growth features

Details of the studied zircons (Electronic Appendix 3) are discussed more generally here. Most zircons show magmatic corrosion on crystal faces and depending on its degree the grains range from euhedral, through subhedral to anhedral shapes (Fig. 4a). The 3-D SEM imaging of Yarrowitch zircons reveals that many have extensive corrosion, removing pre-existing crystal faces and producing undulose and highly pitted surfaces (Fig. 4b). This leaves finely etched, mostly spherical pits and a highly pimpled surface (Fig. 4c). Even crystals with prominent faces still show highly corroded or pitted surfaces (Fig.4d). Some grains exhibit sharp angular, euhedral short negative crystals (Fig. 4e), which may represent prismatic mineral grains dissolved out by magmatic action. Similar strong magmatic resorption is also evident in Podgelbanochny zircons, in which crystals have prismatic and pyramidal faces dominated by {101} forms with an elongation ratio of about 1:2 (Akinin et al. 2004).

Table 2 Zircon Fission Track Analyses (ages in Ma)

Sample number	Relative age group	No. of grains	Ns (av.)	Ni (av.)	Na (av.)	U ppm (av.)	RHOs (× 10n)	RHOi (× 10n)	F.T. Age ± error
YAR Z1-4	Old (low U)	6	182	126	137	96	2.322×10^6	2.882×10^6	65.3 ± 7.8
	Old (high U)	6	208	122	183	183	2.435×10^6	1.673×10^6	57.7 ± 6.2
	Intermediate	4	170	176	138	138	2.993×10^6	3.142×10^6	40.8 ± 4.6
	Young	1	128	2598	300	754	6.780×10^5	1.376×10^7	2.1 ± 0.2
YAR Z1-4	Old	4	P (χ^2) 8 %; Pooled age 62 ± 3 Ma						
	Old	10	P (χ^2) 7–12 %; Pooled age 55 ± 3 Ma						
	Intermediate	2	P (χ^2) 85 %; Pooled age 40 ± 3 Ma						
TC[1]		11	3	69	76	56	6.447×10^4	1.532×10^6	2.7 ± 1.7
MML Z	Old	1	6	11	100	6	9.534×10^4	1.748×10^5	38.3 ± 19.4
	Intermediate	9	3	19	100	10	4.061×10^4	2.966×10^5	10.8 ± 7.2
	Young	14	7	142	100	75	1.056×10^5	2.249×10^6	3.5 ± 2.2
GNV Z1-3	Young	20	1.4	5.3	100	47	2.225×10^4	8.346×10^5	1.1 ± 0.2
BHS Z1	Older (?)	11	28	263	100	211	4.383×10^5	4.172×10^6	4.3 ± 1.0
	Younger (?)	6	11	180	100	158	1.430×10^5	2.655×10^6	2.4 ± 0.7
	Combined	17	P (χ^2) 0.7 %; Pooled age 3.8 ± 0.2 Ma						
PBY Z1	One Group	57	202	185	94	4.875×10^5	1.735×10^6	12.1 ± 0.5	
			P (χ^2) 87.7 %; Pooled age 12.1 ± 0.5 Ma						

From Geotrack Reports for the Australian Museum, # 344 409 901. Analysts P.F. Green & I.R. Duddy. [1] Tobins Camp, Yarrowitch, Sutherland (1993). Errors on ages 1-sigma and on pooled ages 2-sigma. Standards and induced track densities were measured on external detector faces, fossil track densities on internal mineral surfaces. Ages were calculated using Zeta = 87.7 ± 0.8 for dosimeter glass U3. Ns, No. of spontaneous tracks. Ni, No. of induced tracks. Na, area units of counted tracks. RHOs, spontaneous track density, RHOi, induced track density. RHO_D, induced track density/cm^2 ($RHO_D = 9.619 \times 10^5$ for YAR Z1-4, GNV Z1-3, BHSL Z1, PBV Z1 and $= 1.605 \times 10^6$ for MML Z)

Table 3 SHRIMP U-Pb data for zircons

Grain spot	% $^{206}Pb_c$	U_{ppm}	Th_{ppm}	$^{232}Th/^{238}U$	$^{206}Pb^*_{ppm}$	$^{206}Pb^*/^{238}U$	±%	Total ^{206} Pb	U/±%	Total ^{206}Pb	Pb/±%	$^{206}Pb/^{238}U$ Age (Ma) ±2σ	
WRT Z1													
1.1	0.15	58	26	0.46	1.96	0.0393	1.0	25.4	1.0	0.0524	2.3	249	3
2.1	0.08	542	473	0.90	3.34	0.0072	0.7	139.2	0.7	0.0476	1.5	46.1	0.4
3.1	0.25	26	6	0.25	0.93	0.0408	2.3	24.5	2.2	0.0534	2.6	258	9
4.1	0.06	56	19	0.34	1.86	0.0385	1.8	26.0	1.8	0.0516	1.8	244	6
YAR Z5a													
1.1	0.55	388	318	0.85	4.03	0.0120	2.1	82.7	2.0	0.0519	4.7	77.1	2.3
2.1	0.61	179	111	0.64	1.50	0.0097	1.6	102.4	1.6	0.0521	5.8	62.3	1.4
3.1	1.02	286	194	0.70	2.35	0.0095	1.5	104.7	1.4	0.0553	4.9	60.6	1.3
4.1	–	211	173	0.85	1.80	0.0100	1.6	100.5	1.5	0.0466	5.7	63.9	1.4
5.1	–	66	30	0.46	0.59	0.0104	2.6	96.5	2.5	0.0422	10	66.9	2.4
6.1	1.06	96	49	0.52	0.78	0.0094	2.3	105.2	2.2	0.0556	8.7	60.4	2.0
YAR Z5b													
1.1	−0.18	710	879	1.28	6.06	0.0100	1.5	100.6	1.5	0.0458	2.9	63.9	1.3
2.1	0.51	168	137	0.85	1.42	0.0098	2.2	101.5	2.2	0.0513	5.8	62.9	1.4
YAR Z5c													
1.1	0.16	632	879	1.44	5.35	0.0098	1.3	101.4	1.3	0.0486	3.1	63.2	1.2
1.2	0.31	279	222	0.82	2.38	0.0099	2.0	100.8	2.0	0.0498	4.3	63.4	1.3
2.1	0.23	312	377	1.25	2.61	0.0097	1.8	102.7	1.8	0.0491	4.5	62.4	1.8
YAR Z5d													
1.1	0.28	284	289	1.05	2.51	0.0103	1.1	97.0	1.1	0.0495	2.4	65.9	1.0
1.2	0.81	86	40	0.48	0.76	0.0102	1.5	97.2	1.5	0.0537	4.1	65.5	1.4
MML Z1													
2.1	5.38	17	4	0.23	0.051	0.0034	11.2	277.1	10.0	0.0890	42.0	22.0	3.5
3.1	4.27	19	5	0.26	0.062	0.0037	5.2	255.7	4.7	0.0803	20.7	24.1	1.8
4.1	1.91	30	6	0.22	0.099	0.0038	8.3	258.3	8.0	0.0616	25.5	24.4	2.8
4.2	−1.20	26	6	0.23	0.101	0.0046	7.7	221.6	7.5	0.0371	34.7	29.4	3.3
BHSL Z4													
1.1	2.16	103	50	0.50	0.054	0.0006	4.1	1649.6	3.9	0.0632	14.3	3.8	0.23
1.2	1.98	68	26	0.40	0.033	0.0006	5.6	1751.2	5.2	0.0617	24.7	3.6	0.28
2.1	3.39	310	268	0.90	0.135	0.0005	3.6	1967.6	3.5	0.0729	8.4	3.2	0.21
2.2	6.03	105	46	0.45	0.053	0.0006	4.3	1694.1	3.9	0.0937	12.4	3.6	0.21
3.1	0.35	292	154	0.55	0.168	0.0007	2.4	1497.9	2.3	0.0489	10.5	4.2	0.16
3.2	2.03	196	97	0.51	0.112	0.0006	3.0	1501.2	2.8	0.0622	11.4	4.0	0.18
GNV Z4													
3.1	34.40	85	47	0.57	0.010	0.0001	13.3	7035	6	0.3177	15.7	0.6	0.11
3.2	24.89	70	38	0.56	0.011	0.0001	9.2	5580	5	0.2426	14.8	0.9	0.11
4.1	84.57	27	11	0.42	0.005	0.0000	95	4395	6	0.7138	11.0	0.2	0.22
PBV Z1a													
3.1	0.62	791	1378	1.80	1.18	0.0017	2.0	577.7	2.0	0.0512	6.9	11.1	0.31
4.1	–	193	181	0.97	0.31	0.0019	3.4	540.1	3.2	0.0419	19.4	12.0	0.60
4.2	0.61	267	300	1.16	0.46	0.0020	3.0	502.2	2.9	0.0511	13.3	12.7	0.50
PBV Z1b													
1.1	2.67	131	158	1.24	0.21	0.0018	3.3	549.8	3.0	0.0674	14.9	11.4	0.37
2.1	0.74	98	112	1.19	0.14	0.0017	4.2	600.9	3.8	0.0521	27.6	10.6	0.44
3.1	4.83	79	84	1.11	0.13	0.0019	4.4	513.5	3.8	0.0844	17.9	11.9	0.52
PBV Z1c													
1.1	–	63	59	0.96	0.096	0.0018	4.9	568.0	4.8	0.0297	26.8	11.6	0.79

Table 3 (continued)

Grain spot	% $^{206}Pb_c$	U_{ppm}	Th_{ppm}	$^{232}Th/^{238}U$	$^{206}Pb^*_{ppm}$	$^{206}Pb^*/^{238}U$	±%	Total ^{206} Pb	U/±%	Total ^{206}Pb	Pb/±%	$^{206}Pb/^{238}U$ Age (Ma) ±2σ	
2.1	3.93	50	45	0.94	0.069	0.0015	7.4	621.4	7.0	0.0773	23.1	10.0	1.04
3.1	–	50	44	0.92	0.071	0.0018	6.9	596.8	6.8	0.0091	92.1	11.3	1.09
3.2	12.20	42	37	0.91	0.072	0.0018	7.0	495.6	5.5	0.1426	19.8	11.4	1.13
4.1	3.09	54	51	0.99	0.082	0.0017	5.1	558.8	4.6	0.0706	24.2	11.2	0.81
5.1	3.92	37	32	0.89	0.058	0.0017	6.6	556.8	5.7	0.0772	33.0	11.1	1.04

Errors are 2-sigma; Pb_c and Pb* indicate the common and radiogenic portions, respectively. (1) Common Pb corrected by assuming $^{206}Pb/^{238}U$-$^{207}Pb/^{235}U$ age-concordance

ppm = ppm wt

The CL imaging shows that most analysed grains have magmatic growth zoning, as coarser to finer oscillatory zones and sector zones (Fig. 4d–f, best seen in Fig.4d). They generally lack inherited cores or metamorphic or hydrothermal rims found in zircons from metamorphosed igneous-sedimentary complexes (Maidment et al. 2005).

Geochronology

Fission track dating

Results (Table 2) indicate multiple thermal annealing events in some zircon suites, mostly Australian. Previous data on Weldborough zircons indicated a resetting event at 46–47 Ma (Khin Zaw et al. 2006). The Yarrowitch results suggest resetting events of 63 ± 3 age zircons at ~ 55 and 40 Ma, and possibly 2–3 Ma (similar to the nearby Tobins Camp event; Sutherland 1993). Mount McLean suggests two main resetting events at ~ 11 and 4 Ma involving 22–29 Ma zircons. The new FT data further supports scenarios of repeated thermal transport of zircons during eruptive episodes within Australian volcanic basalt fields (Sutherland and Fanning 2001).

The Asian-Russian FT ages are younger than most Australian FT ranges and indicate thermal transport ages close to the zircon formation ages of ~1 Ma at Ghia Nghia, ~3–4 Ma at Ban Hui Sai and ~12 Ma at Podgelbanochny. The U contents in zircons in the FT analysis show low av. U (<60 ppm) for the Mount McLean, Tobins Camp and Gia Nghia suites and moderately high av. U (>90 ppm) in the other suites.

U –Pb dating

The SHRIMP II data (Table 3; Figs. 5 a–f) show that Weldborough (WRT Z1) includes older zircons (249 ± 5 Ma) with relatively low U (26–58 ppm), Th (6–26 ppm) and Th/U (0.25–0.46) and younger zircons (46 ± 1 Ma) much higher in U (542 ppm), Th (473 ppm) and Th/U (0.90). The older age is typical of many Weldborough zircons on the basis of previous SHRIMP I dating (290 ± 25 to 208 ± 10 Ma; Khin Zaw et al. 2006). The younger geochemically distinct zircon has a U–Pb age closely related to the basaltic resetting event at 46–47 Ma.

Yarrowitch zircons (YAR Z5a–d) suggest multiple formation ages. A zircon with higher U (388 ppm), Th (318 ppm) and Th/U (0.85) gave the oldest age (77 ± 2 Ma) age. Zircons with lower U (<300 ppm), Th (<200 ppm) and Th/U (0.46–0.85) gave a spread of ages (67 ± 2 – 60 ± 1 Ma) and overlap with a SHRIMP formation age of 66 ± 2 Ma found for young reset zircons in the area with a FT age of ~ 3 Ma (Sutherland 1993). Mount McLean zircons (MML Z1) range from 24 ± 2.0 to 22.0 ± 3.5 Ma, but the ages are within uncertainty of each other. These low U (17–30 ppm), Th (4–6 ppm) and Th/U (0.22–0.26) zircons clearly formed before thermal resetting events at 11 and 4 Ma (FT ages).

The Asian–Russian zircons gave younger ages than for Australian suites. Gia Nghia zircons (GNV Z4) gave uncorrected Th- disequilibrium U–Pb ages from 0.9 ± 0.1 to 0.2 ± 0.2 Ma and have relatively low U (<85 ppm), Th (<47 ppm) and Th/U (0.42–0.59) values. The 0.9 Ma age lies within error of the pooled FT age of 1.1 ± 0.2 Ma. Ban Huai Sai zircons (BHSL Z4) range in age from 4.2 ± 0.1 to 3.2 ± 0.1 Ma and overlap the FT ages. These zircons range into higher U (68–310 ppm), Th (26–268 ppm) and Th/U (0.40–0.90) than for Gia Nghia zircons. Podgelbanochny zircons (PBV Z1a–c) gave ages from 10 ± 1 to 12 ± 1 Ma, and lie within error of the FT age. They show higher U (37–791 ppm), Th (32–1378 ppm) and Th/U (0.89–1.80) than do Gia Nghia and Ban Huai Sai zircons.

Geochemistry

The EMP analyses for Yarrowitch zircons (Electronic Appendix 5) show Hf substituting for Zr (HfO_2 0.76–1.25 wt%). The Hf/Zr ratios (av. 0.015–0.020) are typical of magmatic zircons in undersaturated to intermediate felsic rocks (Deer et al. 1982). Lesser substitutions include P, Ce, Th and U and Th/U ratios increase with Hf/Zr ratios.

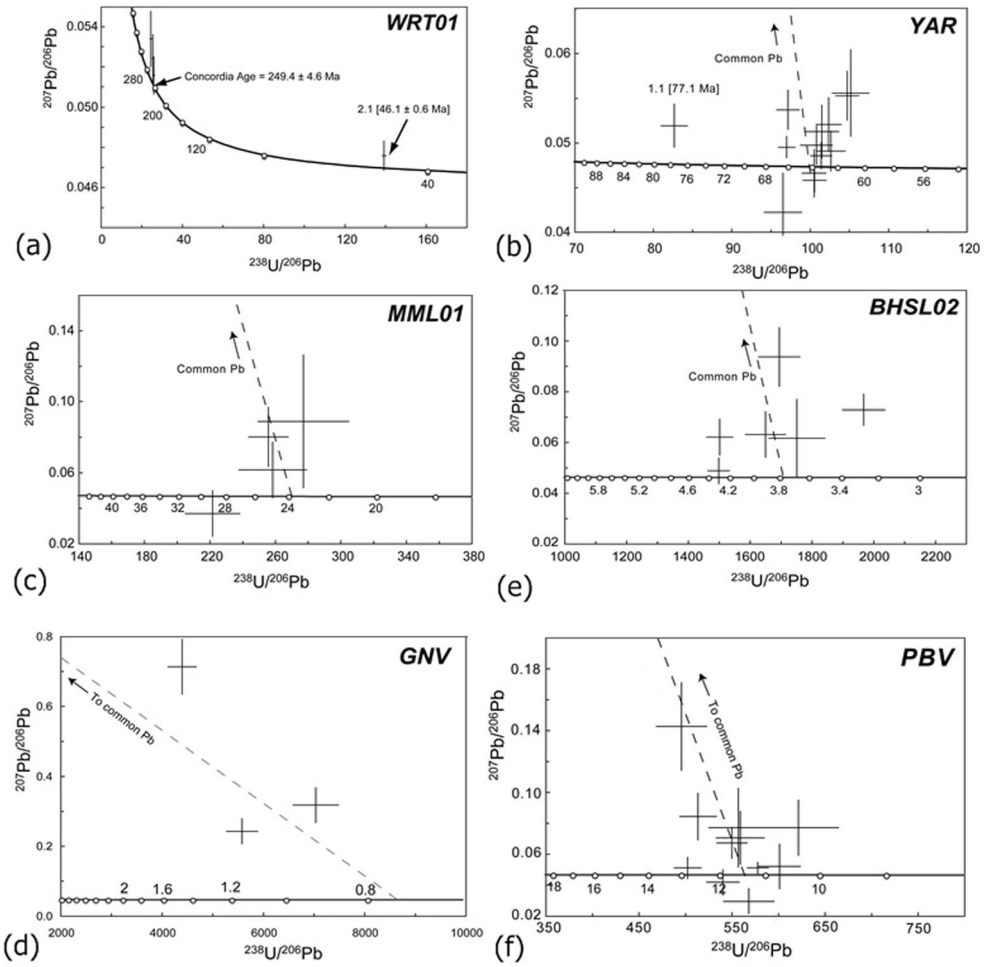

Fig. 5 Tera-Wasserburg U–Pb concordia diagrams for zircon megacrysts. **a** Weldborough, NE Tasmania (WRT01) **b** Yarrowitch, New South Wales (YAR) **c** Mount McLean, Queensland (MML01) **d** Gia Nghia, Dak Nong, Vietnam (GNV) **e** Ban Huai Sai, Laos (BHSL02) **f** Podgelbanochny, Primorye Russia (PBV)

The LA-ICP-MS trace element concentrations (ppm) in the zircons (Electronic Appendix 6) suggest three main groupings. Weldborough, Yarrowitch and Podgelbanochny have very low to low Sr, La and Pr (<0.1– <1 ppm), moderate Ce, Nd, Sm, and Eu (up to 100 ppm) and high Y, Dy, Er, Yb, Hf, Th and U (>100 ppm). Ghia Nghia and Ban Huai Sai differs in their low Nd, Eu and Ta (<1 ppm) and only moderate Yb, Dy, Er, Th and U (up to 100 ppm). Mount McLean zircons have low Ce (0.35–0.73 ppm) and Sm (0.13–0.99 ppm) and higher Ta (up to 1.51 ppm). In total av. REE contents (ppm), younger Weldborough is highest (1907), Yarrowitch (825), Pogelbanochny (844) and Ban Huai Sai (513) are moderately high, older Weldborough (212 ppm) and Gia Nghia (198) are moderate and Mount McLean is lowest (73). The megacrysts generally increase in Th with U, when Th/U ratios are <1 (Electronic Appendix 7a, b). When Th and U levels both exceed 400 ppm, Th/U ratios exceed 1 (younger Weldborough and rare Yarrowitch and Podgelbanochny

Table 4 Zircon O isotope values ($\delta^{18}O$, V-SMOW ‰), megacrysts and composites

Material/locality	Individual crystal/colour/zone (no.		
D53800. Zircon megacrysts, Yarrowitch, NSW	G3 pink (3)	G4 yellow (4)	G2 green (4)
	4.3–5.6 (av. 5.0)	4.0–5.6 (av. 4.6)	4.4–4.5 (av. 4.4)
D53795. Zircon-magnetite composite, Riamukka, NSW	Zoned main core (7)	Outer rim zone (5)	
	5.1–6.1 (av. 5.7)	5.2–6.2 (av. 5.5)	
D53796. Zircon-magnetite-sapphire xenolith, Thailand,	Large zoned crystal (13)	Small zoned crystal (5)	
	6.9–9.4 (av. 8.4)	7.9–8.4 (av.8.1)	

Analyst G. Giuliani

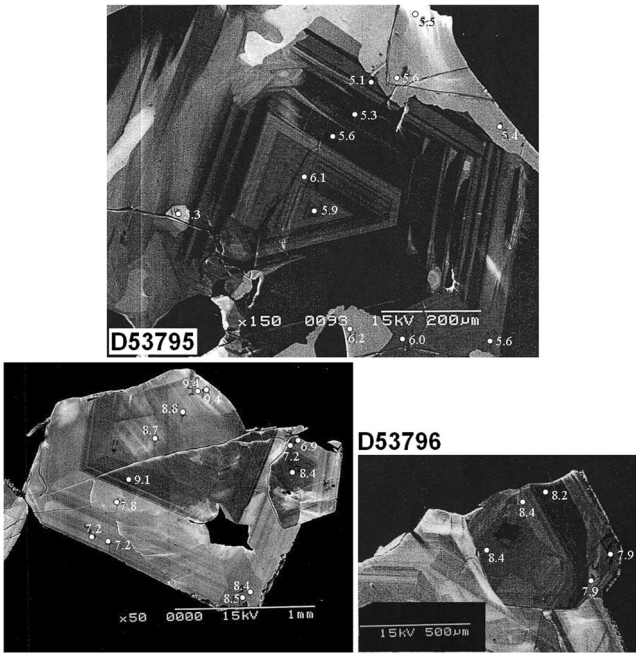

Fig. 6 Cathodoluminescence and SEM images showing oxygen isotope values for: zircon-magnetite composite, Riamukka, New South Wales (D53795); zircon-magnetite-sapphire xenolith, Khao Wu, Chanthaburi-Trat , Thailand (D53796)

megacrysts). The Riamukka composite zircon (Electronic Appendix 8a, b) has a similar though separate Th/U trend, with higher U, Th, Th/U, La, Ce and REE.

The Nb and Ta values and Nb/Ta ratios in the zircons show two main trends, groups with low Nb (1–7 ppm) and Ta (1–3 ppm) and Nb/Ta ratios (1–3) and groups with higher Nb (7–48 ppm), Ta (3.5–21 ppm) and Nb/Ta ratios (2.5–4). The more depleted group includes older Weldborough, Mount McLean, Ghia Nghia, Ban Huai Sai and some Yarrowitch and Pogelbanochny subgroups. The more enriched group includes younger Weldborough, Yarrowitch and Podgelbanochny subgroups. The two sets of values may relate to differences in the source magma compositions. The lower Nb, Ta, Nb/Ta may typify less fractionated, Si-poor melts and higher values more

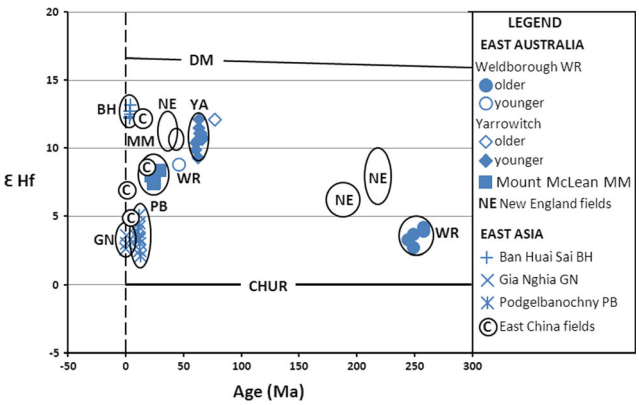

Fig. 7 Epsilon Hf versus U–Pb age, plot of east Australian and Asian megacrysts in relation to CHUR and DM isotopic reservoirs

fractionated and higher Si melts (Belousova et al. 2002). Oxidation effects in melts may also play a part, as Ta^{4+} ion oxidizes more readily than the Nb^{4+}, giving a smaller Ta^{5+} ion that preferentially substitutes into the Zr lattice site. Nb-rich source compositions and other factors may also control Nb-Ta and Zr-Hf fractionation during zircon crystallization, such as mass dependant fractionation, electron configuration control and metasomatic processes (Hui et al. 2011; Van Lichtervelde et al. 2011).

Chondrite-normalised average REE arrays for the zircon suites (Electronic Appendix 9) include some comparative arrays. East Australian arrays (a) include older and younger Weldborough and other Australian arrays. The Asian-Russian arrays (b) are further compared with arrays from several potential magma sources.

Oxygen isotope ($\delta^{18}O$) analyses

The zircon $\delta^{18}O$ (‰) values are given in Table 4 and are shown in relation to growth zoning in some examples (Fig. 6). Values are lowest in the Yarrowitch megacrysts (4.0–5.6 ‰, av.4.4‰) and marginally higher (5.1–6.2, av. 5.6 ‰) in the Riamukka composite zircon (Ce/Ce* 1.8, Eu/Eu* 0.70). These values overlap the range for Phanerozoic mantle-generated zircon (4.5–5.7 ‰; Valley 2003). Zircon crystals in a Thailand sapphire-magnetite xenolith have higher values (6.9–9.4 ‰), more typical of crustal associations. The wider range of values in larger crystals, beyond analytical uncertainty, suggest changes in source conditions during growth.

$^{176}Hf/^{177}Hf$ and $^{176}Lu/^{177}Hf$ analyses

These measured isotopic ratios and the calculated initial εHf values using the U–Pb ages of the grains are listed in Electronic Appendix 10 and plotted in Fig. 7. The Lu–Hf CHUR (chondrite uniform reservoir) line comes from Bouvier et al. (2008) using parameters $^{176}Lu/^{177}$ Hf CHUR present day = 0.0336 ± 1 and $^{176}Hf/^{177}Hf$ CHUR present day = 0.282785 ± 11 and the ^{176}Lu decay constant of 1.865×10^{-11} from Scherer et al. (2001). The Depleted Mantle (DM) reference line comes from Griffin et al. (2000).

The lowest εHf values (<5) lie towards the CHUR reference line (εHf 0) and include older Weldborough (~2.5–4.5), Gia Nghia (~2–4) and Pogelbanochny (~1.5–5) zircons (Fig. 7). The highest εHf values (9–14) lie towards the DM reference line and include Yarrowitch (9–12) and Ban Huai Sai (12–14) zircons (Fig. 7). Mount McLean (~7–8) and younger Weldborough (~8.5) zircons represent intermediate εHf values among the suites. In comparison, these new Lu–Hf results overlap previous results from the Australian-Asian region, which includes zircon megacryst suites from New

Table 5 Summary of geochemical ratios, ZIP zircon groups

Field	Th/U	Ce/Ce*	Eu/Eu*	(Yb/Sm)N
Weldborough				
Group 1	0.26	14.29 (3.46)	0.75 (0.94)	36.7
Group 2	0.36–0.48	2.26–7.03 (8.16–40.48)	0.71–0.81 (0.92–0.93)	24.0–66.7
Group 3	1.18	20.58 (76.40)	0.65 (0.77)	50.1
Yarrowitch				
Group 1	0.47–0.69	3.72–43.88 (10.36–125.92)	0.55–0.80 (0.64–1.00)	84.9–184
Group 2	0.63–1.27	22.08–116.21 (94.50–315.11)	0.63–0.79 (0.81–0.92)	82.2–141
Group 3	0.91–1.42	18.33–69.02 (46.85–210.59)	0.64–2.41 (0.81–0.94)	76.9–121
Mount McLean				
Group 1	0.19	29.6 (35.69)	0.79 (1.11)	98.6
Group 2	0.42–0.44	4.26–6.76 (11.84–22.88)	0.84–0.91 (1.01–1.07)	22.9–23.5
Group 3	0.23	15.69 (29.59)	0.72 (3.55)	96.3
Gia Nghia				
Group 1	0.43–0.61	3.44–21.38 (17.60–58.78)	0.69–0.78	32.5–80.3
Group 2	0.62	3.60 (13.05)	0.76 (0.89)	35.3
Ban Huai Sai				
Group 1	0.41–0.53	25.9–34.75 (69.56–79.52)	0.30–0.32 (0.39–0.42)	162–182
Group 2	0.51–0.97	5.35–12.68 (14.48–33.96)	0.20–0.34 (0.24–0.41)	77.2–85.9
Podgelbanochny				
Group 1	0.89–1.02	11.51–64.44 (33.95–126.43)	0.74–0.78 (0.84–0.91)	25.6–50.5
Group 2	0.93–1.21	10.78–85.06 (26.15–256.94)	0.54–0.75 (0.67–0.88)	30.1–78.7
Group 3	1.03–1.66	100.25-132.69 (173.39-409.16)	0.52-0.61 (0.66-0.73)	44.7-92.8
Group 4	1.31	95.08 (317.68)	0.30 (0.38)	77.5

Ce/Ce*, Eu/Eu* after Belousova et al. (2002). (Ce/ Ce*, Eu/Eu*) after Hoskin & Schaltegger (2003)

England, New South Wales (Abduriyim et al. 2012) and eastern China (Yu et al. 2010).

Discussion

To test the megacryst groups for potential linear geochemical trends, regression lines were calculated for plots between selected trace element pairs (not figured). Linear regressions for Th vs U and Y vs U for Gia Nghia and Podgelbanochny zircons show high correlation coefficients (>0.93). Weldborough, Yarrowitch and Ban Huai Sai results suggest some linear behaviour, but include disparate groupings. Mount McLean Th vs U plots show little linear coherence, although their Y vs U plots do so, providing ambiguous results. Suites with the two strongest linear trends (GNV, PBV) differ in their respective gradients for Th vs U (0.66 *cf* 1.42) and Y vs U (9.51 *cf* 5.55), suggesting different geochemical controls within their respective crystallisation. Podgelbanochny Th vs U and Y vs U gradients resemble the Yarrowitch gradients suggesting similar geochemical conditions in their evolution. The strongly linear suites (GNV, PBV) show Th vs U gradients that approach 1, while the Y vs U gradients are variable. None of the suites approach the high Th/U ratios (>3) in zircons from mantle diopside-phlogopite veins related to carbonatitic kimberlites (Dawson et al. 2001). Plots for other element pairs, show little linear behaviour, particularly in relation to Hf. These variations suggest that the linear trends are linked to specific substitution sites, but mostly not coupled with Hf–Zr substitution.

The total REE, Y and U concentrations and Ce and Eu relationships within each suite suggest some discrete subgroups exist (Electronic Appendix 11). These subgroups suggest direct correspondences between REE, Y and U values within suites, although gaps between subgroups vary in extent. The Ce and Eu relationships probably relate to anomalies that developed within REE patterns due to valency/oxidation and ionic size substitution effects during crystallization (Hoskin and Schaltegger 2003). These anomalies are measured relative to adjoining chondrite- normalised (CN) REE values, La and Pr for Ce (Ce/Ce*) and Sm and Gd for Eu (Eu/Eu*). Two methods are used to calculate the anomaly size. Either the Ce and Eu values are divided by averaged adjacent element values (e.g. Belousova et al. 2002), or by the square root of the multiplied adjacent element values (e.g. Hoskin and Schaltegger 2003). This can give differences in the individual anomaly values (see Table 5), so that the method used needs citing for making literature comparisons. Results with

Table 6 Ti ppm values (LA-ICP-MS) and T°C estimates (Ferry & Watson 2007), zircon megacrysts

Australian Megacrysts (Grain.spot) ppm					
WRT Z1	YAR Z5 a	YAR Z5 b	YAR Z5 c	YAR Z5 d	MML Z1
(1.1) 1.93	(1.1) 3.69	(1.1) 6.81	(1.1) 4.44	(1.1) 2.92	(1.1) 5.32
(1.2) 1.35	(2.1) 3.11	(2.1) 4.88	(2.1) 3.42	(1.2) (*45.47*)	(2.1) 2.18
(2.1) 2.52	(3.1) 3.50		(3.1) 5.91		(3.1) 4.41
(3.1) 2.78	(4.1) 1.17		(4.1) 5.13		(4.1) 3.75
(4.1) 0.76	(5.1) 2.15				(5.1) 4.47
	(6.1) 1.52				
	(7.1) 2.27				
Ti 0.76–2.78	1.17–3.69	4.88–6.81	3.42–5.91	2.92–45.47	2.18–5.32
T°C 550–638	578–660	682–711	654–699	642–(*911*)	620–690
Asian-Russian Megacrysts (Grain.spot) ppm					
BHS Z2	GNV Z4	PBVa	PBVb	PBVc	
(1.1) 3.34	(1.1) 4.78	(1.1) 6.13	(1.1) 9.23	(1.1) 7.90	
(1.2) 15.9	(2.1) 6.48	(2.1) 9.16	(2.1) 7.94	(2.1) 12.17	
(2.1) 6.09	(2.2) 7.11	(3.1) 4.59	(3.1) 7.50	(3.1) 6.63	
(2.2) 3.83	(3.1) 7.11	(4.1) 5.22	(4.1) 6.88	(4.1) 7.60	
(3.1) 1.43	(4.1) 3.47			(5.1) 8.30	
(3.2) 1.73	(4.2) 5.03				
Ti 1.43–15.9	3.47–7.11	4.59–9.16	6.88–9.23	6.63–12.17	
T°C 591–791	655–715	667–738	712–738	708–765	

La values below detection limit make calculations of Ce anomalies problematic.

In this study, Pr correlates well with Nd and Sm over two orders of magnitude on log-log plots, whereas La values do not correlate with Pr or any other REE. Some La values seem too high either due to an analytical problem or contamination, so that calculating Ce/Ce* would give minimum values. Estimates, however, can be approached using extrapolation of Ce* from a curve fit through the other REE. In addition, recent experimental work on Ce and Eu anomalies in natural zircon revealed complex temperature and chemical inheritance effects in source melts which need consideration in interpreting Ce and Eu anomaly patterns (Trail et al. 2012). Calculated Ce/Ce* anomalies for zircon increase with higher oxygen fugacity and decrease with crystallisation temperature, so provides less precise oxidation data than given by other fugacity monitors. In contrast, Eu/Eu* in the melt is controlled by both oxygen fugacity and inherited Eu/Eu* and Eu depletion neither needs later feldspar (particularly plagioclase) crystallization nor a temperature relationship.

Source magmas for ZIP megacrysts

Various elemental ratios such as Zr/Hf, Th/U, Hf/Y and Nb/Ta and CN-multi-element and REE patterns in zircons (Table 5; Electronic Appendix 7– 9, 11–14) help to constrain likely source magma affinities. The Zr/Hf ratios generally decrease with fractionation, so that Yarrowitch megacrysts (HfO_2 from 0.8 to 1.1 wt %) would suggest moderately evolved magmas within the ranges shown by carbonatitic, syenitic and granite pegmatitic hosts (Hoskin and Schaltegger 2003). The Hf values in the studied zircon megacrysts (4250 to 7300 ppm) exceed those for zircon 'megacrysts' in nepheline syenite xenoliths from the French Massif Central alkali basalts (2810 to 3880 ppm; Paquette and Mergoil-Daniel 2009). However, as Hf-enriched zircons (13,315 to 16,705 ppm) also occur in nepheline syenite xenoliths in Bohemian alkali basalts (Ulrych and Uher 1999), Hf and Zr/Hf values seem unreliable indicators of precise zircon megacryst source magma compositions. Most Th/U ratios in the studied zircons exceed 0.5, typical of many silicate melts. Mount McLean has lower ratios (0.19 to 0.44), suggesting a separate affinity, but within ranges among rarer magmas, such as kimberlitic and mafic N-MORB, anatectic granite and trondhjemite melts (Belousova et al. 2002; Schulz et al. 2006).

Zircon Hf and Y correlations are used to delineate affinities for magmatic zircons (Pupin 2000; Belousova et al. 2002), although xenocrysts from basalts may mask their initial affinities. The ZIP megacryst plots spread across a Hf (wt %)–Y (ppm) diagram (Electronic Appendix 12) and overlap plots for known mantle zircon megacrysts (NE Italian basalts; Visonà et al. 2006). Plots, however, may incorporate strong zoning in zircon, which will blur Hf–Y trends. They mostly concentrate away from limits for typical kimberlitic, carbonatitic, lamproitic, doleritic and granitoid zircon fields, but show marginal overlaps into kimberlitic (Mt McLean) and granitoid

(Yarrowitch, Ban Huai Sai, Podgelbanochny) fields. The main East Australian field overlaps a New Zealand field, while zircon composites range from granitoid (Riamukka) to carbonatitic and ultrabasic (Khao Wua) affinities.

The classification and regression trees (CART) applications of Belousova et al. (2002) uses further zircon geochemistry to characterize zircon petrological fields, using various plots such as Y values against heavy to mid-REE ratios (Electronic Appendix 13a, b). Applying such plots to ZIP suites (a) focuses on their enrichment in HREE (Yb/Sm >10). Yarrowitch, Ban Huai Sai and composite zircons have higher Yb/Sm (~>100) than the other suites, with Ghia Nghia, Weldborough and New Zealand having least Yb/Sm enrichment. In the combined Y–Yb/Sm plots, Mt McLean, older Weldborough and Gia Nghia fields overlap into kimberlite, carbonatite and syenite fields, while the other suites trend into the granitoid field. Another instructive example plots Y values against Nb/Ta ratios, which reflect two levels of Nb-Ta values in the ZIP results. This diagram (Electronic Appendix 13b) reinforces the general ZIP groupings shown by the Y–Yb/Sm plots. Ce/Ce* vs Eu/Eu* plots also find use in CART correlations, but need cautious interpretation as they involve complications related to inherited source and thermal restrictions (Trail et al. 2012).

The application of CART analysis to zircons may generate some anomalies, as a descriptive rather than a fully prescriptive classification (Hoskin and Schaltegger 2003). Further analyses from specific hosts, however, has widened its scope (Veevers et al. 2006; E. A. Belousova pers. comm. 2012). CART analysis, nevertheless, can yield a spread of results from one host rock, e.g. zircons from Antarctic nepheline syenite gave carbonatitic, mafic, syenitic and granitoid origins (Veevers et al. 2006). Explanations advanced for such spreads were gaps in the CART data-base or multiple xenocrysts which was considered unlikely. Another possibility raised here is redistribution of incompatible elements in the zircons under tectonic effects (Timms et al. 2006; Reddy et al. 2009), as that host rock had undergone Palaeozoic transtension and subduction events. Such redistributions are less likely to affect the post-orogenic ZIP suites in this study.

A CART tree matched against the separate ZIP subgroups (Table 5) suggests that some include mixed sources. Weldborough (sg 1–3) gave carbonatitic, syenitic, granitoid and basaltic matches, Yarrowitch (sg 1–3) were all basaltic, Mount McLean (sg 1–3) included kimberlitic and carbonatitic, Gia Nghia (sg 1–2) were mostly syenitic but also basaltic, Ban Huai Sai (sg 1–2) were all basaltic, Podgelbanochny (sg 1–4) were basaltic and larvikitic. Further CART-based diagrams (Veevers et al. 2006) were used to compare zircons in ZIP megacrysts, composites and inclusions in sapphire and mantle-derived zircons from the Italian Venetian and West Eger basalt provinces (Electronic Appendix 13, 14). Most ZIP suites generated mixed petrological assignments. However, significantly different petrological peaks appeared in younger Weldborough (60 % granitoid), in Yarrowitch, Ban Huai Sai and Pogelbanochny (25–41 % lamproitic), in Mt McLean and Gia Nghia (37–60 % kimberlitic, 16–36 % syenitic), and in Ban Huai Sai (56 % mafic) suites.

In general ZIP megacrysts and composites reflect a wide range of low-silica alkaline, K-rich and alkaline mafic, and intermediate to felsic magmas. Zircon inclusions in sapphire extends into high-Hf –enriched melts (Sutherland et al. 2015). In some cases, CART correlations can highlight marked distinctions within ZIP suites sampled from alluvial sources, as at Weldborough where younger zircon gave a strong granitoid signal in contrast to other source signals from older megacrysts.

Temperature relationships for ZIP megacrysts

Application of Ti-in-zircon thermometry to zircons include some uncertainties (Ferry and Watson (2007), particularly in estimating activities of SiO_2 and TiO_2 and pressure in the source melts. Pressure effects were estimated at 50 ° C/ GPa, but is probably twice this at GPa <1, based on Ti substitutions in both Si and Zr sites (Ferriss et al. 2008). For ZIP megacrysts, the precise TiO_2 and SiO_2 activities in the crystallising medium are unknowns. At 750 ° C, changing TiO_2 activity from 1.0 to 0.5 will increase *T* by 60–70 ° C and changing SiO_2 activity likewise will decrease *T* by a similar amount. As TiO_2 activities in silicate melts are rarely < 0.5, these corrections should be relatively small for calculated TiO_2: SiO_2 at 1:1 (Table 6). Since the *T* estimates incorporate most of the above uncertainties, any notable differences between the zircon sets are probably real.

Averaged estimates for older Weldborough (WRT 1, 3, 4), younger Weldborough (WRT2) and Yarrowitch orange-brown (YAR5a) zircons lie in the range *T* ~550–640 ° C. Intermediate *T* ranges between 650 and 700 ° C are given for Mount McLean (MM1), Yarrowitch white (YAR5b), Yarrowitch red (YAR5c), Ban Huai Sai (BHS2) and Gia Nghia (GNV4) megacrysts and higher *T* of ~700–750 ° C for Podgelbanochny (PBVa, b, c) megacrysts . These *T* estimates overlap those for other Australasian megacrysts (Sutherland and Meffre 2009; Abduriyim et al. 2012; Sutherland et al. 2014, 2015) and late-crystallizing *T* ranges for a variety of ultramafic, alkaline mafic and felsic magmas (Ferreira et al. 2002; Litvinovsky et al. 2002; Fall et al. 2007; Page et al. 2007). The Riamukka composite zircon (Ti 12–23 ppm; 755–830 ° C) and Lava Plains mantle-zircon included in sapphire (Ti 7– 24; 715–830 ° C; Sutherland et al. 2015) give higher *T* than most ZIP megacrysts, but overlap estimates for West Eger rift mantle-zircons (725–810 ° C; Siebel et al. 2009).

Genetic conditions for zircon megacryst formation

This study and cited literature suggest a variety of source melts and *P–T–X* conditions produced the ZIP associations. Most ZIP megacrysts lack significant Eu depletions, so that plagioclase fractionation was not significant in their genesis, although some noticeable depletions appear in Ban Huai Sai and in the REE-enriched Podgelbanochny megacrysts. Marked depletions, however, appear in high-U Gloucester Tops megacrysts (Sutherland and Fanning 2001). Usually, a strong chemical differentiation appears between the megacrystic zircon and zircon included in sapphire, as the latter shows higher Hf, Th and U and often notable Eu depletion indicating separate chemical and probably different *P–T–X* processes (Izokh et al. 2010). However, in some cases the processes may overlap. In the Denchai gem field, Thailand (Limtrakun 2002) and in SE Saxony, Germany (Seifert et al. 2008), the zircon megacrysts and zircon inclusions in sapphire overlap in HfO_2 (<1.6 wt %) and indicate closer genetic ties. In zircon (± corundum)–bearing albitite dykes in Pyrenean mantle peridotites, zircon in the corundum–bearing dykes shows higher Hf, U, Th and REE than zircon in the dykes without corundum (Monchoux et al. 2006; Pin et al. 2006). This was attributed to differences in relative CO_2 and H_2O contents in the crystallizing magmas within a similar *P–T* regime.

The Ce and Eu anomalies in zircon suites reflect valency changes related to changes of redox conditions during partial mantle melting, melt interactions and eruptive processes, but can guide mantle or crustal assignments to zircons (Li et al. 2000). Similar Eu/Eu*– Ce/Ce* plots for ZIP and mantle-derived zircons show many congregate along an extended mantle array line (Electronic Appendix 14). Some suites (Ban Huai Sai, Khoa Wua composite) lie within a crust-mantle transitional zone. Combining $\delta^{18}O$ for ZIP megacrysts (Nechaev et al. 2009) with Eu/Eu*–Ce/Ce* can further reinforce such assignments, as $\delta^{18}O$ values for Yarrowitch, Podgelbanochny and Riamukka composite (4.2–6.2‰) overlap typical ranges in values for rocks encountered within mantle peridotites (Zheng et al. 2005a). Higher $\delta^{18}O$ values for Khao Wua and some Lava Plains zircons (6.9–10.5‰; Sutherland et al. 2015) are more typical of crustal ranges. Generally lower $\delta^{18}O$ combined with + εHf values (2–14) for many ZIP zircons, however, suggest a significant mantle role in their genesis. Thus, ZIP suites crystallized at mantle to crustal levels, over a wide *P–T–X* range. The subdued negative Eu anomalies in many of their REE patterns negates widespread feldspar (plagioclase) fractionation within their crystallizing sources, even though felsic compositions are indicated. This may favour crystallization under mantle pressures beyond plagioclase stability limits, ~ 0.8 GPa in fertile mantle lherzolite (Borghini et al. 2009).

Zircon crystallised at mantle levels would occur at or above the expected ambient geotherm *T* at that depth. Some estimated *T* ranges for ZIP megacrysts seem low for a mantle geotherm origin, although the higher ranges would match *T* intersections at 25 to 35 km depth, typical of Moho depths in eastern Australia (Collins et al. 2003). Given uncertainties in Ti-in-zircon and xenolith thermo-barometry *P–T* estimates and in sources for Eu and Ce anomalies, these parameters only give provisional lithospheric correlations for ZIP megacrysts.

Synthesis of the ZIP zircon megacryst formation

The genesis of zircon-bearing megacryst suites along western Pacific margins involves temporal and geodynamic aspects. Temporal inputs include times of zircon formation and transport in basaltic volcanism, while geodynamic inputs involve the roles of rifting, mantle upwells, sea floor spreading and subduction events. While local tectonic settings play a role, repeated formation/ transport of such zircon megacrysts along the continental western Pacific margin suggests that a wider petrological process links them together. Further studies of ZIP genesis and distribution will help test the overall modelling (Electronic Appendix 16).

Temporal ZIP relationships

Dual U–Pb and FT dating on the zircons indicate multiple ages of formation and then thermal annealing events. The time gaps between formation and later resetting can range from near-coeval, to several Ma, extending up to 20 Ma, and in some cases between 40 and 100 Ma and in the most extreme case over 200 Ma (older Weldborough). Some sites include multiple ages of zircon formation and repeated basaltic transport that extended over spans of 55 to 70 Ma (Electronic Appendix 15). Such prolonged residence before basaltic ascent is known elsewhere (Siebel et al. 2009). Young zircon formation in eastern Australia (~0.3 Ma, Th-corrected U–Pb age, Bullenmerri maar; Hiess et al. 2012; Sutherland et al. 2014) and Asia (~0.2 Ma, U–Pb age, Gia Nghia; this paper) suggest that potential active zircon-forming processes remain under young basalt areas.

The $^{176}Hf/^{177}Hf$ values in zircons in relation to their initial source values and radiogenic inputs can be tracked using their U–Pb ages combined with ^{176}Lu–^{176}Hf isotopic decay effects (Simonetti and Neal 2010; Matteini et al. 2010). This method was applied to ZIP megacrysts from East China (Qiu et al. 2007; Yu et al. 2010) and East Australia (Abduriyim et al. 2012) and add to results for comparison here (Fig. 7). All these ZIP suites show + εHf, which probably signifies inputs from re-fertilization events within depleted mantle (Yu et al. 2010). The lowest + εHf values (2–5; older Weldborough, Gia Nghia, Podgelbanochny), also provide the highest Tcrustal (0.68–1.02 Ga) and TDM (0.48–0.76 Ga) model ages. The Tcrustal

ages are only applicable if crustal components entered source melts, while the TDM ages mark minimum ages of mantle protolith events.

The oldest model ages (older Weldborough zircons) may relate to complex basement fragmentation, migrations and impacts of the late Proterozoic exotic Tasmanian-Selwyn block and its early Paleozoic impacts with SE Australian terranes (Cayley 2011). In Asia-Russia, model Tcrustal (0.68–0.86 Ga) and TDM (0.48–0.59 Ga) ages (Gia Nghia, Pogelbanochny) coincide with break-up of the supercontinent Rodinia, opening the PaleoAsian and PaleoPacific oceans (0.9 to 0.7 Ga), major mantle re-fertilization (Dobretsov et al. 2003; Kovach et al. 2011) and early Phanerozoic fragmentations and collisions along margins of the South China and China-Korean blocks (Lin et al. 2008; Derbeko 2013).

The younger Tcrustal (0.32–0.56 Ga) and TDM (0.26–0.38 Ga) ages in eastern Australia (Weldborough, Yarrowich, Mt McLean) reflect continental source inputs after major separation from Rodinia (post- 0.58 Ga) with subsequent collisional accretions (Fergusson et al. 2007). These accretionary orogenic phases formed the Lachlan, New England and Hodgkinson Fold Belts, providing the settings for later ZIP sites. In SE Asia, young Tcrustal (0.20–0.26 Ga) and TDM (0.14–0.16) ages (Ban Huai Sai) probably reflect sources developed after significant late Permian andesitic/subduction in the area at ~ 0.25 Ga (Phommakaysone 2012).

In comparisons with other ZIP studies (Fig. 7), New England, Australian older zircons (~0.17 to 0.24 Ga) show lower εHf (6–10) and higher TDM (0.47–0.56 Ga) and Tcrustal (0.63–0.82 Ga) ages than younger New England zircons (0.037–0.045 Ga; εHf 10–14; TDM 0.16–0.29 Ga; Tcrustal (0.23–0.45 Ga). The older model ages match proposed source inputs linked to orogeny along the post-Rodinia Pacific margin (Fergusson et al. 2007), while the younger ages overlap late orogenic activity and the Mesozoic break-up of eastern Gondwana (Scheibner 1999). The East China mantle-derived zircons (εHf + 3–14) overlap the range of εHf for young ZIP suites in this study. The highest εHf (+11.8–13.4) at Muling suggests more depleted mantle existed there, while TDM in the south-trending suites (0.48–0.32 Ga) suggests progressive modifications of mantle sources took place since early Paleozoic time.

Overall, the ZIP model ages suggest diverse contributions from heterogeneous mantle events, complex crustal continental break-ups and multiple orogenic re-workings along an extended Indo-Pacific margin. For the suites in the higher εHf ranges, the TDM model ages may represent the most appropriate source correlations.

Geodynamic influences

The ZIP intraplate basalts formed along past spreading basins, older and more distant from subduction zones for Australian than for Asian-Russian basins. More prevalent western Pacific back-arc and sea-floor basins than developed on eastern Pacific subduction margins may reflect relative ages of the subducting slabs (Nishimura 2002). Dehydration in older, cooler, western slabs may favour thermal convection mantle wedges behind the arcs, where hot, thin and weak lithosphere contributes long-term term heat (Hyndman et al. 2005). The continental margins are currently moving NNE for Australia (5–7 cm/y; Tregoning 2003) and ESE for Asia-Russia (1–2 cm/y; Kreemer et al. 2003). They have migrated from their original mantle upwelling positions, pre-52 Ma for Australia (Gaina et al. 1998) and pre-12–16 Ma for Asia-Russia (Sibuet et al. 2001; Ismail-Zadeh et al. 2013). Such original thermal rift and metasomatic zones may influence later overlying geodynamic processes (Rasskazov et al. 2003; Lei and Zhao 2005; Finn et al. 2005). Whether rift-spreading basaltic ZIP magmatism in eastern Australia (Vasconcelos et al. 2008; Sutherland et al. 2012) and ZIP magmatism along Asian-Russian marginal basins (Graham et al. 2008) are closely similar or distinctly different needs consideration. Residual slabs from Pacific subduction lie under some basalt fields (Replumaz et al. 2004; Lei and Zhao 2005). Metasomatic pyroxenites and hornblendite veins in mantle wedge peridotite were proposed for generating intraplate alkali basalts in China (Zhang et al. 2009; Dai et al. 2014) and such veins would provide Zr-bearing melts for zircon crystallization. The two ZIP regions are considered separately.

Eastern Australia

Lithosphere along this margin migrates over residual slabs to depths > 200 km and borders an extensive mantle thermal zone 100 to 300 km deep under the Southwest Pacific back-arc system, developed after changes in Phoenix Plate subduction at ~ 100 Ma (Sdrolias et al. 2003; Rey and Müller 2008). This triggered prolonged spreading, basaltic volcanism and ZIP development (Sutherland et al. 2012; 2014). Deep slabs that passed below Australian lithosphere (Schellart et al. 2009, Schellart and Spakman 2015) may have affected earlier basaltic and ZIP generation. Later advance of NE Australian lithosphere over slabs from New Guinea convergence has generated flexural stresses and mantle melting since 10 Ma (Dyksterhuise and Müller 2008), which incorporates ZIP developments (Mt McLean, Lava Plains; this study; Sutherland et al. 2015). Some ZIP basalts generated since 35 Ma mark lithospheric migration over large seismically slow asthenospheric perturbations at depths between 200 and 600 km (Kennett and Abdullah 2011; Sutherland et al. 2012; 2014). Migration of eastern Australian lithosphere since late Cretaceous time (Schellart and Spakman 2015), when traced over long-term asthenospheric upwelling (Electronic Appendix 1) provides a cohesive model for numerous basaltic episodes and accessory ZIP developments.

In a model that linked gem megacryst formation to passage over thermal upwells interacting with metasomatized mantle (Sutherland et al. 1998; Sutherland and Fanning, 2001), zircon-corundum crystallizing melts develop early and late in the magmatic process and some ascend into crustal levels. Continued lithospheric traverse over such upwells can deliver multiple-aged ZIP sites in local basalt fields over periods exceeding 55 Ma. Clearly, Australian ZIP genesis involved a geodynamically-sustained thermal process.

Eastern Asia-Russia

This region also shows significant mantle thermal upwells, but cooler mantle underlies former spreading floors and regions with westerly subducting slabs from adjacent convergent boundaries (Electronic Appendix 1). Several rift and back arc spreading events formed the Gulf of Thailand, South China Sea, Japan Sea and Sea of Okhotsk (Verzhbitsky and Kononov 2006; Yin 2010; Zhao et al. 2010; Ismail-Zadeh et al. 2013; Zahirovic et al. 2014). These events initiated Neogene intraplate basaltic volcanism and its scattered ZIP sites (Yin 2010). Most SE Asian ZIP sites correlate with post-rift stages of Gulf of Thailand basins and NW–SE and N–S faulting in the Lampang–Chein Rai and Indochina plates (<12 Ma ; Shoup et al. 2012). South China Sea rifting marked a significant thermal feature and most East China ZIP basalts post-date cessation of the spreading phase (~20.5 Ma; Cullen et al. 2010). Far East Russian ZIP sites mostly post-date Japan Sea and Sea of Okhotsk spreading (<15 Ma; Nechaev et al. 2009; Yin 2010).

The former spreading floors have migrated ESE with lithospheric plate motion (2 to 4 cm/y; Ismail-Zadeh et al. 2013), so that the initial asthenospheric thermal zones went below subcontinental lithosphere, to form basalt magmas and attendant ZIP sites. Active slabs subducted along the Japan arc descend through thermal upwelling zones below Primore basalt fields and the large Changabi volcano where slabs reach depths below 410 km (Lei and Zhao 2005; Ismail-Zadeh et al. 2013). Breaching of the slab under Changabai allowed escape of subsidiary thermal upwells. Within the mantle upwells, imposed slabs affected mantle melting and major lithospheric faults tap basaltic magmas, to contribute to ZIP distribution in these regions.

Conclusions

Zircon megacrysts occur as derived xenocrysts from Mesozoic-Cenozoic intraplate alkaline basalts, adjacent to rift/spreading basins along West Pacific continental margins. This 12,000 km N–S zone of multiple zircon crystallizations yields U–Pb formation ages from 250 to < 1 Ma and ZFT reset ages from 205 to <1 Ma.

The zircons largely lack inherited cores or metamorphic overgrowths and suggest diverse lithospheric, mostly magmatic origins. Mineral inclusions and trace element patterns indicate derivation from ultramafic to felsic source magmas. Crystallization *T*, based on Ti-in-zircon thermometry, ranges from 550 to 830 ° C.

Main element parameters such as Hf and Zr/Hf values for the zircons form initial, but partly unreliable indicators of source magmas. Trace element parameters such as U, Th and U/Th values indicate some systematic magmatic trends, but also irregular exceptions, between megacryst suites.

The Y and total REE values vary considerably in megacryst suites and provide some constraints in assigning zircons to specific source magmas. Use of Ce/Ce*/ Eu/Eu* plots help to relate zircons to mantle or crustal magma sources, but source complexities and a broad transitional overlap limit exact interpretations.

Isotopic O ($\delta^{18}O$) and Hf ($^{176}Hf/^{177}Hf$) values for zircons suggest mantle and crustal sources, including metasomatized mantle. Initial εHf values (+2–14) related to zircon ages suggest magma sources inherited inputs from a range of mantle (TDM 0.14–0.76 Ga) and continental (Tcrustal 0.20–1.02 Ga) model age events.

Combined U–Pb and ZFT age-dating, trace element, O and Hf-Lu isotopic geochemistry, crystal form and Ti-in-zircon thermometry analysis on zircons from ZIP basalt fields gives a wide data base to consider their genesis. The present study suggests their origin is related to multiple factors, rather than a simple origin.

The ZIP zone reflects intraplate magmatism along continental margins to former spreading rifts. East Australian zones developed earlier and farther from bounding subduction zones than did most Asian-Russian sites. Lithospheric motions over asthenospheric upwells and back-arc slab insertions contributed to ZIP genesis.

Acknowledgments This zircon megacryst (ZIP) study is dedicated to Rex Prider, former Professor of Geology, University of Western Australia, for his pioneer studies on lamproitic rock suites in Australia.

The project was supported by Australian Museum Geodiversity Research Centre funding, SEM imaging was facilitated by Sue Lindsay, Australian Museum, SHRIMP age dating and LA-ICP-MS facilities at Research School of Earth Sciences, Australian National University, Canberra, assisted by Chuck Magee, Charlotte Allen and Steve Eggins, ZFT dating guided by Paul Green, Geotrack International, Melbourne, EMP analyses at School of Sciences, University of Western Sydney, guided by Adam McKinnon, and Hf-Lu isotope analytical facilities at Earth Sciences, University of Melbourne. Ion-microprobe O isotope analysis used facilities in Centre National de la Recherche Scientifique, University of Lorráine, Nancy, France. Data calculations were assisted by Elena Belousova, Earth Sciences, Macquarie University, Sydney, and plate motion reconstructions for East Australia and East Asia benefitted from support by Sabin Zaharovic, Maria Seton and Dietmar Müller, EarthByte Group, School of Geosciences, University of Sydney.

Sampling at Yarrowitch, New South Wales, was assisted by Ray Andrews and Joe Terp, at Central-Western Victoria by Julian Hollis, and from Primore deposits, Russia, by Alexander Khanchuk and Sergei

Vysotskiy, Far East Geological Institute, Vladivostok. Zircons in the Australian Museum collections were provided by Ross Pogson, Collection Manager, from Ban Huai Sai, Laos and Khao Wau, Thailand, by Robert Coenraads, Sydney, George Bosshart, Gübelin Lab, Lucerne, Switzerland and Ponsong Vichit, Bangkok, Thailand.

Script and figure preparation assistance involved Roger Springthorpe, Australian Museum, Francesca Kelly, Sydney and Jacqueline Timms, University of Western Sydney. Early drafts of the paper were read by Sebastien Meffre, Earth Sciences, University of Tasmania and Larry Barron, University of New South Wales, Sydney. Further constructive comments came from Richard Hinton, School of Geosciences, University of Edinburgh and Elena Belousova, Earth Sciences, Macquarie University. Three anonymous reviewers provided constructive improvements to the paper.

References

Abduriyim A, Sutherland FL, Belousova EB (2012) U–Pb age and origin of gem zircon from the New England sapphire fields, New South Wales, Australia. Aust J Earth Sci 59:1067–1081

Akinin VV, Visotskiy SV, Mazdab FK, Mille E, Wooden JL (2004) Shrimp dating of zircon from the Podgelbanochny alkali basalt volcano in Primore, Russian Far East: Application to genesis of megacrysts. In: Khanchuk AI, Gonevchuk GA, Mitrokhin AN, Simanenko LF, Cook NJ, Seltmann R (eds) Metallogeny of the Pacific Northwest: Tectonics, magmatism and metallogeny of active continental margins. Dalnauka, Vladivostok, pp 323–326

Ashwal LD, Armstrong RA, Roberts RJ, Schmitz MD, Corfu F, Hetherington CJ, Burke K, Gerber M (2007) Geochronology of zircon megacrysts from nepheline-bearing gneisses as constraints on tectonic setting: implications for resetting of the U-Pb and Lu-Hf isotopic systems. Contrib Mineral Petrol 153:389–403

Barr SM, Cooper MA (2013) Late Cenozoic basalt and gabbro in the subsurface in the Phetchabun Basin, Thailand: implications for Southeast Asian Volcanic Province. J Asian Earth Sci 76:169–184

Belousova EA, Griffin WL, O'Reilly SY, Fisher NI (2002) Igneous zircon: trace element composition as an indicator of source rock type. Contrib Mineral Petrol 143:602–622

Birch WD, Barron LM, Magee C, Sutherland FL (2007) Gold- and diamond-bearing White Hills Gravel, St Arnaud district, Victoria: age and provenance based on U–Pb dating of zircon and rutile. Aust J Earth Sci 54:609–628

Borghini G, Fumagalli P, Rampone E (2009) The stability of plagioclase in the upper mantle: subsolidus experiments on fertile and depleted lherzolite. J Petrol 51:229–254

Bouvier A, Vervoot JD, Patchett PJ (2008) The Lu–Hf and Sm–Nd isotope composition of CHUR constraints from unequilibrated chondrites and implications for the bulk composition of terrestrial planets. Earth Planet Sci Lett 273:48–57

Cayley RA (2011) Exotic crustal block accretion to the eastern Gondwanaland margin in the Late Cambrian–Tasmania, the Selwyn Block, and implications for the Cambrian–Silurian evolution of the Ross, Dalmerian, and Lachlan orogens. Gondwana Res 19:628–649

Chashchin AA, Martynov YA, Rasskazov SV, Maksimov SO, Brandt IS, Saranina EV (2007) Isotopic and geochemical characteristics of the Late Miocene subalkali and alkali basalts of the southern part of the Russian Far East and the role of continental lithosphere in their genesis. Petrology 15(6):575–598

Cherniak DJ, Watson EB (2001) Pb diffusion in zircon. Chem Geol 172: 5–24

Cocherie A, Fanning CM, Jezequel P, Robert M (2009) LA-MC-ICPMS and SHRIMP U– Pb dating of complex zircons from Quaternary tephras from the French Massif Central: magma residence time and geochemical implications. Geochim Cosmochim Acta 73: 1095–1108

Coenraads RR, Vichit P, Sutherland FL (1995) An unusual sapphire-zircon-magnetite xenolith from the Chanthanburi Gem Province, Thailand. Min Mag 59:465–479

Collins CDN, Drummond BJ, Nicoll MG (2003) Crustal thickness patterns in the Australian continent. Geol Soc Aust Spec Pub 22 and Geol Soc Amer Spec Pap 372: 121–128

Corfu F, Hanchar JM, Hoskin PWO, Kinny P (2003) Atlas of zircon textures. In: Hanchar JM, Hoskin PWO (eds) Zircon, vol 53, Rev Mineral Geochem., pp 469–500

Crawford AJ, Meffre S, Symonds PA (2003) 120 to 0 Ma tectonic evolution of the southwest Pacific and analogous geological evolution of the 600 to 220 Ma Tasman Fold Belt System. Geol Soc Aust Spec Pub 22 and Geol Soc Amer Spec Pap 372: 383–403

Cullen A, Reemst P, Henstra G, Gozzard S, Ray A (2010) Rifting of the South China Sea: new perspectives. Pet Geosci 16:273–282

Dai L-Q, Zhao ZF, Zhang Y-F (2014) Geochemical insights into the role of metasomatic hornblendite in generating alkali basalts. Geochim Geophys Geosyst 15:3762–3779

Davis DW, Barr SM (1995) U–Pb dating of 1–10 Ma mantle zircon megacrysts from southeast Asia. Victoria '95. Geol Assoc Can/ Mineral Assoc Can Ann Meet, Final Prog and Abst 20: A-23

Dawson JB, Hill PG, Kinny PD (2001) Mineral chemistry of a zircon-bearing, composite, veined and metasomatised upper-mantle peridotite xenolith from kimberlite. Contrib Mineral Petrol 140:720–733

Deer WA, Howie RA, Zussman J (1982) Zircon. Rock-forming Minerals. Volume 1A, 2nd Edit, Orthosilicates. Geol Soc, London: 418–442

Derbeko I (2013) The region of matching of Central Asian Mobile Belt and Pacific Mobile Belt. Int J Geosci 4:605–610

Dobretsov NI, Buslov MM, Vernikovsky VA (2003) Neoproterozoic to early Ordovician evolution of the Paleo-Asian Ocean: implications to the break-up of Rodinia. Gondwana Res 6:143–159

Dyksterhuise S, Müller RD (2008) Cause and evolution of intraplate orogeny in Australia. Geology 36:495–498

Fall A, Bodnar RJ, Szabo C, Pál-Molnár E (2007) Fluid evolution in the nepheline syenites of the Ditrau Alkaline Massif, Transylvania, Romania. Lithos 95:331–345

Fergusson C, Henderson RA, Fanning CM, Withnall IW (2007) Detailed zircon ages in Neoproterozoic to Ordovician siliciclasticrocks, northeastern Australia: implications for the tectonic history of the East Gondwana continental margin. J Geol Soc Lond 164:215–225

Ferreira MAF, Ferreira VP, Sial AN, Pimentel MM (2002) Origin and intensive parameters in the crystallisation of ultrapotassic Syenites: the Serra Do Man Pluton, Northeastern Brazil. Gondwana Res 5: 275–285

Ferriss EDA, Essene EJ, Becker U (2008) Computational study of the effect of pressure on the Ti-in-zircon geothermometer. Eur J Mineral 20:745–755

Ferry JM, Watson EB (2007) New thermodynamic model and revised calculations for the Ti-in-zircon and Zr-in-rutile thermometers. Contrib Mineral Petrol 154:429–437

Finn CA, Müller RD, Panter KS (2005) A Cenozoic diffuse alkaline magmatic province (DAMP) in the south Pacific without rift or plume origin. Geochem Geophys Geosyst 6, Q02005. doi:10.1029/2004GC000723

Gaina C, Müller RD, Royer J-Y, Stock J, Hardbeck J, Symonds P (1998) The tectonic history of the Tasman Sea: a puzzle with 13 pieces. J Geophys Res 103:12413–12433

Garnier V, Ohenstetter D, Guiliani G, Fallick AE, Phan Trong T, Hoang Quang V, Van Pham L, Schwarz D (2005) Basalt petrology, zircon ages and sapphire genesis from Dak Nong, southern Vietnam. Min Mag 69:21–38

Giuliani G, Chaussidon M, Schubnel H-J, Piat DH, Rollion-Bard C, France-Lanord C, Giard D, de Narvaez D (2000) Oxygen isotopes

and emerald trade routes since antiquity. Science 287(5453):631–633

Giuliani G, Fallick AE, Garnier V, France-Lanord C, Ohnenstetter D, Schwarz D (2005) Oxygen isotope composition as a tracer for the origins of rubies and sapphires. Geology 33(4):249–252

Giuliani G, Fallick AE, Ohnenstetter D, Pegere G (2009) Oxygen isotope composition of sapphires from the French Massif Central: implications for the origin of gem corundum in basaltic fields. Miner Deposita 44:221–231

Graham I, Sutherland L, Zaw K, Nechaev V, Khanchuk A (2008) Advances in our understanding of the gem corundum deposits of the West Pacific continental margins intraplate basaltic fields. Ore Geol Rev 34(1–2):200–215

Griffin WL, Pearson NJ, Belousova E, Jackson SE, van Achterbergh E, O'Reilly SY, Shee SR (2000) The Hf isotope composition of cratonic mantle: LAM-MC-ICPMS analysis of zircon megacrysts in kimberlite. Geochim Cosmochim Acta 64:133–147

Groat LA (ed) (2014) Geology of gem deposits. Second Edition. Miner Assoc Can Short Course 44: 1–405

Gübelin EJ (ed) (1982) World map of gem deposits. Swiss Gemmol Soc, Berne

Guo J, O'Reilly SY, Griffin WL (1996a) Corundum from basaltic terrains: a mineral inclusion approach to the enigma. Contrib Mineral Petrol 122:368–386

Guo JF, O'Reilly SY, Griffin WL (1996b) Zircon inclusions in corundum megacrysts in alkali basalts I. Trace element geochemistry and clues to the origin of corundum megacrysts in alkali basalts. Geochim Cosmochim Acta 60:2347–2363

Hall RS, Spakman W (2003) Mantle structure and tectonic evolution of the region north and east of Australia. Geol Soc Aust Spec Publ 22 and Geol Soc Am Spec Pap 372: 361–381

Hanchar JM, Hoskin PWO (eds) (2003) ZIRCON. Rev Miner Geochem 53: 1–500

He H, Zhu R, Saxton J (2011) Noble gas isotopes in corundum and peridotite xenoliths from Eastern North China Craton: implication for comprehensive refertilization of lithospheric mantle. Phys Earth Planet Inter 189:185–191

Hiess J, Condon DJ, McLean N, Noble SR (2012) $^{238}U/^{235}U$ systematics in terrestrial uranium-bearing minerals. Science 335:1610–1614

Hinton RW, Upton BGJ (1991) The chemistry of zircon: variations within and between large crystals from syenite and alkali basalt xenoliths. Geochim Cosmochim Acta 55:3287–3302

Hoang N, Flower M (1998) Petrogenesis of Cenozoic basalts from Vietnam: implications for origins of a diffuse igneous province. J Petrol 39:369–395

Hollis JD, Sutherland FL (1985) Occurrence and origins of gem zircons in eastern Australia. Rec Aust Mus 36:299–311

Hoskin PWO, Schaltegger U (2003) The composition of zircon and igneous and metamorphic petrogenesis. In: Hanchar JM, Hoskin PWO (eds) Zircon, vol 53, Rev Mineral Geochem., pp 27–62

Hui H, Niu Y, Zhidan Z, Huixin H, Dicheng Z (2011) On the enigma of Nb-Ta and Zr-Hf fractionation – A critical review. J Earth Sci 22:52–66

Hyndman RD, Currie CA, Mazzotti SP (2005) Subduction zone backarcs, mobile belts, and orogenic heat. GSA Today 15(2):4–10

Ismail-Zadeh A, Hoda S, Tsepelev I (2013) Linking mantle upwelling with the lithosphere descent and the Japan Sea evolution: a hypothesis. Sci Rep 3: doi:10.1038/srep001137

Itoh Y, Uno K, Arato H (2006) Seismic evidence of divergent rifting and subsequent deformation in the southern Japan Sea, and a Cenozoic tectonic synthesis of the eastern Eurasian margin. J Asian Earth Sci 27:933–942

Izokh AE, Smirnov SV, Egorova VV, Anh TT, Kovyazin SV, Phuong NT, Kalinina VV (2010) The condition of formation of sapphire and zircon in the areas of alkali basaltoid volcanism in Central Vietnam. Russ Geol Geophys 51:719–753

Kennedy AK, Wotzlaw J-F, Schaltegger U, Crowley JL, Schmitz M (2014) Eocene zircon reference material for microanalysis of U–Th–Pb isotopes and trace elements. Can Mineral 52:409–421

Kennett BLN, Abdullah A (2011) Seismic wave attenuation beneath the Australian margin. Aust J Earth Sci 58:285–295

Khamloet P, Pisutha-Arnond V, Sutthirat C (2014) Mineral inclusions in sapphire from the basalt-related deposit in Bo Phloi, Khanchanburi, western Thailand: indication of their genesis. Russ Geol Geophys 55:1087–1091

Khanchuk A (2001) Pre-Neogene tectonics of the Sea-of-Japan region: a view from the Russian side. Earth Sci (Chikyu Kagaku) 55:275–291

Khanchuk A, Zalishchak B, Pakhamova V, Odarichenko E, Sapin V (2003) Genesis and gemmology of sapphires from the Nezametnoye deposit, Primore Region, Russia. Aust Gemmol 21: 369–375

Kirkland CL, Smithies RH, Taylor RJM, Evans N, McDonald B (2014) Zircon Th/U ratios in magmatic environs. Lithos. doi:10.1016/j.lithos.2014.11.021

Kovach V, Salnikova E, Wang K-L, Jahn B-M, Chiu HY, Reznitskiy L, Kotov A, Izuka Y, Chung S-L (2011) Zircon ages and Hf isotopic constraints and source of metasediments of the Slyudyansky high-grade complex, southeastern Siberia: implication for continental growth and evolution of the Central Asian Orogenic Belt. J Asian Earth Sci 62:18–36

Kreemer C, Holt WE, Haines AJ (2003) An integrated global model of present-day plate motions and plate boundary deformations. Geophys J Int 154:8–34

Lan C-Y, Chung S-L, Ho C-H, Lee T-Y, Wang P-L, Li H, Toan DV (2001) First evidence for Archaean continental crust in northern Vietnam and its implications for crustal and tectonic evolution in Southeast Asia. Geology 29:219–222

Lei J, Zhao D (2005) P-wave tomography and origin of the Changbai intraplate volcano in Northeast Asia. Tectonophysics 397:281–295

Li X-H, Liang X, Sun M, Liu Y, Tu X (2000) Geochronology and geochemistry of single-grain zircons: simultaneous *in-situ* analysis of U-Pb age and trace elements by LAM-ICP-MS. Eur J Mineral 12: 1015–1024

Limtrakun P (2002) Origin and distribution of corundum from intraplate alkali basaltic province in Thailand: Evidence from field and inclusion studies. PhD Thesis, University of Tasmania (unpubl)

Limtrakun P, Zaw K, Ryan CG, Mernagh TP (2001) Formation of the Denchai gem sapphire, northern Thailand: evidence from mineral chemistry and fluid/melt inclusion characteristics. Min Mag 65: 725–735

Lin W, Wang Q, Chen k (2008) Phanerozoic tectonics of South China block: New insights from the polyphase deformation in the Yunkan massif. Tectonics (6):TC6004, 16p

Litvinovsky BA, Jahn M-M, Zanvilevich AN, Saunders A, Poulain S, Kuzmin DV, Reichow MK, Titov AB (2002) Perrogenesis of syenite-granite suites from the Bryansky Complex (Transbaikalia, Russia): implications for the origin of A-type granitoid magmas. Chem Geol 189:105–133

Liu Y, Gao S, Yuan H, Zhou L, Liu X, Wang X, Hu Z, Wang L (2004) U–Pb zircon ages and Nd, Sr, and Pb isotopes of lower crustal xenoliths from North China Craton: insights on evolution of the lower crust. Chem Geol 211:87–109

Maidment DW, Hand M, Williams IS (2005) Tectonic cycles in the Strangways metamorphic complex, Arunta Inlier, central Australia: geochronological evidence for exhumation and basin development between two high-grade metamorphic events. Aust J Earth Sci 52: 205–215

Marshallsea SJ, Green PF, Webb J (2000) Thermal history of the Hodgkinson Province and Laura Basin, Queensland: multiple cooling episodes identified from apatite fission track analysis and vitrinite reflectance data. Aust J Earth Sci 47:779–797

Matteini M, Dantas EL, Piemental MM, Bühn B (2010) U–Pb and Lu–Hf isotope analyses by laser ablation MC-ICP-MS: methodology and application. An Acad Bras Ciênc 82(2):474–491

Metcalfe I (1999) Gondwanaland dispersion and Asian accretion: an overview. In: Metcalfe I, Jishuin R, Charvet J, Hada S (eds) Gondwanaland Dispersion and Asian Accretion. Balkema, Rotterdam, pp 9–28

Mezger K, Krongstad EJ (2004) Interpretation of discordant U–Pb zircon ages: an evaluation. J Metamorph Geol 15:127–140

Miller MS, Kennett BLN, Toy VG (2006) Spatial and temporal evolution of the subducting Pacific plate structure along the western Pacific margin. J Geophys Res 111, B02401. doi:10.1029/2005JB003705

Monchoux P, Fontan F, De Parseval P, Martin RF, Wang RC (2006) Igneous albitite dikes in orogenic lherzolites, western Pyrénées, France: a possible source for corundum and alkali feldspar xenocrysts in basaltic terranes. I. Mineralogical Associations. Can Mineral 44:817–842

Moore ME, Gleadow AJW, Lovering JF (1986) Thermal evolution of rifted continental margins: new evidence from fission tracks in basement apatites from southeastern Australia. Earth Planet Sci Lett 78: 255–270

Mukasa SB, Fisher GM, Barr SM (1996) The character of the subcontinental mantle in Southeast Asia: Evidence from isotopic and elemental compositions of extension-related Cenozoic basalts in Thailand. In: Hart SR, Basu AR (eds) Earth processes: reading the isotopic codes, vol 95, AGU Geophys Monogr., pp 233–252

Nechaev VP, Nechaeva EV, Cashchin AA, Vysotskiy SV, Graham IT, Sutherland FL (2009) New isotopic data on Late Cenozoic age and mantle origin of gem zircon and corundum from placers of Primorye, Russ. Dokl Earth Sci 429A(9):1426–1429

Nishimura S (2002) Why are there no back-arc basins around the eastern Pacific margin? Revis Mexic Cienc Geológ 19:170–174

Okamura S, Arculus RJ, Martynov YA (2005) Cenozoic magmatism of the North-Eastern Eurasian Margin: the role of lithosphere versus asthenosphere. J Petrol 46:221–253

Page FZ, Fu B, Kita NT, Fournelle J, Spicuzza MJ, Schulze DJ, Viljoen F, Basei MAS, Valley JW (2007) Zircons from kimberlite: new insights from oxygen isotopes, trace elements, and Ti in zircon thermometry. Geochim Cosmochim Acta 71:3887–3903

Paquette J-L, Mergoil-Daniel J (2009) Origin and U–Pb dating of zircon-bearing nepheline syenite xenoliths preserved in basaltic tephra (Massif Central, France). Contrib Mineral Petrol 158:245–262

Phommakaysone K (2012) The Geology and Mineral Resources of Lao PDR, Dept Geol Miner Resour, Ministry of Natural Resources and Energy, Lao PDR, pdf.: 1–26

Pin C, Monchoux P, Paquette J-L, Azambre B, Wang RC, Martin RF (2006) Igneous albititic dikes in orogenic lherzolites, Western Pyrénées, France: a possible source for corundum and alkali feldspar xenocrysts in basaltic terranes. II. Geochemical and petrogenetic considerations. Can Mineral 44:843–856

Pisutha-Arnond V, Wasthanakul P, Intasopa S, Griffin WL (1998) Corsilzirspite, a corundum-sillimanite-zircon-hercynite rock: New evidence on the origin of Kanchanaburi sapphire, Thailand. Ninth Regional Congress on Geology, Mineral and Energy Resources of Southeast Asia: 95–96

Pupin JP (2000) Granite genesis related to geodynamics from Hf-Y in zircon. Trans Roy Soc Edinb Earth Sci 91:245–256

Qiu Z, Wu F, Yu Q, Xie L, Yang S (2005) Hf isotopes of zircon megacrysts from the Cenozoic basalts in eastern China. Chin Sci Bull 50(2):2602–2611

Qiu Z, Yang JH, Yang SF, Li CY, Wang Y, Lin WP, Yang XX (2007) Trace element and Hafnium isotopes of Cenozoic basalt-related zircon megacrysts at Muling, Heilongjiang Province, northeast China. Acta Petrol Sin 23(2):481–492

Rasskazov SV, Logachev NA, Kozhevnikov VM, Yanovskaya TB (2003) Multistage dynamics of the upper mantle in eastern Asia: relationships between wandering volcanism and low-velocity anomalies. Russ Dok Earth Sci 390(4):492–496

Reddy SM, Timms NE, Hamilton PJ, Smyth HR (2009) Deformation-related microstructures in magmatic zircon and implications for diffusion. Contrib Mineral Petrol 157:231–244

Replumaz A, Kárason H, van der Hilst RD, Besse J, Tapponnier P (2004) 4-D evolution of SE Asia's mantle from geological reconstructions and seismic tomography. Earth Planet Sci Lett 221(1–4):103–115

Rey PF, Müller RD (2008) Late Cretaceous–Paleocene evolution of the East Gondwana margin, a new dynamic model for the formation of marginal basins. PESA Eastern Australasian Basins Symposium III, Sydney, 14–17 September, 2008: 261–267

Scheibner E (1999) The geological evolution of New South Wales – a brief review. Geol Surv NSW, Sydney 32

Schellart WP, Spakman W (2015) Australian plate motion and topography linked to fossil New Guinea slab below Lake Eyre. Earth Planet Sci Lett 421:107–116

Schellart WP, Kennet BLN, Spakman W, Amaru M (2009) Plate reconstruction and tomography reveal a fossil lower mantle slab below Tasman Sea. Earth Planet Sci Lett 278:143–151

Scherer E, Münker C, Mezger K (2001) Calibration of the Lutecium-Hf clock. Science 27:683–687

Schmitt AK (2006) Laacher see revisited: high spatial –resolution zircon dating indicates rapid formation of a zoned magma chamber. Geology 34:597–600

Schulz B, Klemd R, Brätz H (2006) Host rock compositional controls on zircon trace element signatures in metabasites from the Austroalpine basement. Geochim Cosmochim Acta 70:697–710

Sdrolias M, Müller RD, Gaina C (2003) Tectonic evolution of the southwest Pacific using constraints from backarc basins. Geol Soc Aust Spec Pub 22 and Geol Soc Am Spec Pap 372: 243–359

Seifert W, Rhede D, Tietz O (2008) Typology, chemistry and origin of zircon from alkali basalts of SE Saxony (Germany). N Jb Mineral Abh 184:299–313

Seifert W, Förster H-J, Rhede D, Tietz O, Ulrych J (2012) Mineral inclusions in placer zircon from alkali basalts from the Ohře (Eger) Graben: new data on "strontiopyrochlore". Mineral Petrol 106:39–53

Shor R, Weldon R (2009) Ruby and sapphire production and distribution: a quarter century of change. Gems Gemol 45(4):236–259

Shoup R, Morely RJ, Swiecicki T, Clark S (2012) Tectonostratigraphic framework and Tertiary palaeogeography of Southeast Asia: Gulf of Thailand to South Vietnam Shelf. AAPG Int Conf Exhib, Singapore, Sept 16–19, 2012, Search Discover Art 30246: 1–16

Sibuet J-C, Hsu S-K, Le Pichon X, Le Formal J-P, Reed D, Moore G, Liu C-S (2001) East Asia plate tectonics since 15 Ma: constraints from the Taiwan region. Tectonophysics 344:103–134

Siebel W, Schmitt AK, Danisik M, Chen F, Meier S, Weiss S, Eroglu S (2009) Prolonged mantle residence of zircon xenocrysts from the western Eger rift. Nat Geosci 2:886–890

Simonet C, Paquette JL, Pin C, Lasnier B, Fritsch E (2004) The Dusi (Garba Tula) sapphire deposit, Central Kenya – a unique Pan-African corundum-bearing monozonite. J Afr Earth Sci 38:401–410

Simonetti A, Neal CR (2010) In-situ chemical U-Pb dating, and Hf isotope investigation of megacrystic zircons, Malaita (Solomon Islands): evidence for multiple stage alkaline magmatic activity beneath the Ontong Java Plateau. Earth Planet Sci Lett 295:251–261

Smith MH, Balmer WA (2009) Zircon mining in Cambodia. Gems Gemol 45(2):152–154

Sun Z, Zhong Z, Keep M, Zhou D, Cai D, Li X, Wu S, Jiang J (2009) 3D analogue modelling of the South China Sea: a discussion on breakup pattern. J Asian Earth Sci 34:544–566

Sutherland FL (1993) Late thermal events based on zircon fission track ages in northeastern New South Wales and south eastern Queensland: links to Sydney Basin seismicity. Aust J Earth Sci 40: 461–470

Sutherland FL (1996) Alkaline rocks and gemstones, Australia: a review and synthesis. Aust J Earth Sci 43:323–343

Sutherland FL (2003) 'Boomerang' migratory intraplate Cenozoic volcanism, eastern Australia rift margins and the Indian-Pacific mantle boundary. Geol Soc Aust Spec Pub 22 and Geol Soc Am Spec Pap 372: 203–221

Sutherland FL, Fanning CM (2001) Gem-bearing basaltic volcanism, Barrington, New South Wales: Cenozoic evolution based on basalt K-Ar ages and zircon fission track and U-Pb isotope dating. Aust J Earth Sci 48:221–237

Sutherland FL, Meffre S (2009) Zircon megacryst ages and geochemistry, from a placer, Dunedin volcanic area, eastern Otago, New Zealand. N Z J Geol Geophys 52(3):185–194

Sutherland FL, Hoskin PWO, Fanning CM, Coenraads RR (1998) Models of corundum origin from alkali basalt terrains: a reappraisal. Contrib Mineral Petrol 133:356–372

Sutherland FL, Bosshart G, Fanning CM, Hoskin PWO, Coenraads RR (2002a) Sapphire crystallisation age and origin, Ban Huai Sai, Laos: age based on zircon inclusions. J Asian Earth Sci 20:841–849

Sutherland FL, Graham IT, Pogson RE, Schwarz D, Webb GB, Coenraads RR, Fanning CM, Hollis JD, Allen TC (2002b) The Tumbarumba basaltic gem field, New South Wales: in relation to sapphire-ruby deposits of eastern Australia. Rec Aust Mus 54:215–248

Sutherland FL, Graham IT, Meffre S, Zwingmann H, Pogson RE (2012) Passive-margin prolonged volcanism, East Australian Plate: outbursts, progressions, plate controls and suggested causes. Aust J Earth Sci 59:983–1005

Sutherland FL, Graham IT, Hollis JD, Meffre S, Zwingmann H, Jourdan F, Pogson RE (2014) Multiple felsic events within post-10 Ma volcanism, Southeast Australia: inputs in appraising proposed magmatic models. Aust J Earth Sci 61:241–267

Sutherland F, Coenraads RR, Abduriyim A, Meffre S, Hoskin PWO, Giuliani G, Beattie R, Wuhrer R, Sutherland GB (2015) Corundum and zircon relationships, Lava Plains gem fields, NE Australia: integrated mineralogy, geochemistry, dating and geographic typing. Mineral Mag 79:545–581

Tietz O, Büchner J (2007) Abundant in-situ zircon megacrysts in Cenozoic basaltic rocks in Saxony, Germany. Z Dt Ges Geowiss 158(2):201–206

Timms NE, Kinny PD, Reddy S (2006) Enhanced diffusion of uranium and thorium linked to crystal plasticity in zircon. Geochem Trans 7: 10

Trail D, Watson EB, Tailby ND (2012) Ce and Eu anomalies as proxies for oxidation state of magmas. Geochim Cosmochim Acta 97:70–87

Tregoning P (2003) Is the Australian Plate deforming? A space geodetic perspective. Geol Soc Aust Spec Pub 22 and Geol Soc Am Spec Pap 372: 41–48

Ulrych J, Uher P (1999) Low-hafnium zircon from alluvial and colluvial placers of northern Bohemia: composition and possible sources. Geol Sudet 32:139–146

Upton BGJ, Hinton RW, Aspen P, Finch A, Valley JW (1999) Megacrysts and associated xenoliths: evidence for migration of geochemically enriched melts in the upper mantle beneath Scotland. J Petrol 40: 935–956

Upton BGJ, Finch AA, Slaby E (2009) Megacrysts and salic xenoliths in Scottish alkali basalts: derivatives of deep crustal intrusions and small melt fractions from the upper mantle. Mineral Mag 73:943–956

Valley JW (2003) Oxygen isotopes in zircon. In: Hanchar JM, Hoskin PWO (eds) Zircon, vol 53, Rev Mineral Geochem., pp 343–385

Van Lichtervelde M, Holtz F, Dziony W, Ludwig T, Meyer H-P (2011) Incorporation mechanisms of Ta and Nb in zircon and implications for pegmatites. Am Minerol 96:1079–1089

Vasconcelos PM, Knessel KM, Cohen BE, Helm JA (2008) Geochronology of the Australian Cenozoic: a history of tectonic and igneous activity, weathering, erosion and sedimentation. Aust J Earth Sci 55:865–914

Veevers JJ (2001) ATLAS of Billion-year earth history of Australia and neighbours in Gondwanaland. GEMOC PRESS, Sydney: 76 p

Veevers JJ, Belousova EA, Saeed A, Sircombe K, Cooper AF, Read SE (2006) Pan-Gondwanaland detrital zircons from Australia analysed for HF-isotopes and trace elements reflect an ice-covered Antarctic provenance of 700–500 Ma age, T_{DM} of 2.0-1.0 Ga, and alkaline affinity. Earth Sci Rev 76:134–174

Verzhbitsky EV, Kononov MV (2006) Geodynamic evolution of the Sea of Okhotsk region from geophysical data. Isvest Phys Solid Earth 42:490–501

Visonà D, Caironi V, Carraro A, Dallai L, Fioretti AM, Fanning M (2006) Zircon megacrysts from basalts of the Venetian Volcanic Province (NE Italy): U–Pb ages, oxygen isotopes and REE data. Lithos 94: 168–180

Vysotskii SV, Shcheka SA, Nechaev VP, Sorok VP, Barkov AV, Khanchuk AI (2002) First finding of sapphire from Cenozoic alkali-basaltic volcanoes in the Primor'e region. Dok Akad Nauk SSR, Earth Sci 387A:1100–1103

Vysotskiy SV, Nechaev VP, Kissin AY, Yakovenko VV, Ignat'ev AV, Velivetskaya TA, Sutherland FL, Agoshkov AI (2015) Oxygen isotopic composition as an indicator of ruby and sapphire origin: a review of Russian occurrences. Ore Geol Rev 68:164–170

Wittwer A, Nasdala L, Wathanachaisaeng B, Bunnag N, Škoda R, Balmer WA, Geister G, Zeug M (2013) Mineralogical characterisation of gem zircon from Ratanakiri, Cambodia. CORALS 2013 (Conference on Raman and Luminescence Spectroscopy in the Earth Sciences), Vienna, Austria, July 3–6, Abst:115–116

Woodhead J, Hergt J, Shelly M, Eggins S, Kemp R (2004) Zircon Hf isotope analysis with an excimer laser, depth profiling, ablation of complex geometries and concomitant age estimation. Chem Geol 2009:1067–1081

Worden JM, Baadsgaard H, Cracknell DN, Krstic D (1996) Major extensional events recorded by zircon xenocrysts from the central Queensland gemfields. Geol Soc Aust Abstr Ser 43:569–573

Yamada R, Tagami T, Nishimura S, Ito H (1995) Annealing kinetics of fission tracks in zircon: an experimental study. Chem Geol 122:249–258

Yim WW-S, Gleadow AJW, Van Moort JC (1985) Fission track dating of alluvial zircons and heavy mineral province on North-East Tasmania. J Geol Soc Lond 142:351–356

Yin A (2010) Cenozoic tectonic evolution of Asia. Tectonophysics 488: 293–325

Yu Y, Xu X, Chen X (2010) Genesis of zircon megacrysts in Cenozoic alkali basalts and the heterogeneity of subcontinental mantle lithosphere, eastern China. Mineral Petrol 100:75–94

Yui T-F, Zaw K, Limkatrun P (2003) Oxygen isotope composition of the Denchai sapphire, Thailand: a clue to its enigmatic origin. Lithos 67: 153–161

Yui T-F, Wu C-M, Limtrakun P, Sricharn W, Boonsoong A (2006) Oxygen isotope studies on placer sapphire and ruby in the Chanthanburi-Trat alkali basaltic gemfields, Thailand. Lithos 86(3–4):197–211

Zahirovic S, Seton M, Müller RD (2014) Cretaceous and Cenozoic tectonic evolution of South East Asia. Solid Earth 5:227–273

Zaw K, Sutherland FL, Dellapasqua F, Ryan CG, Yui T-F, Mernagh TP, Duncan D (2006) Contrasts in gem corundum characteristics, eastern Australian basaltic fields: trace elements, fluid/melt inclusions and oxygen isotopes. Min Mag 70:669–687

Zaw K, Meffre S, Lai C-K, Burrett C, Santosh M, Graham I, Manaka T, Salam A, Kamvong T, Cromie P (2014) Tectonics and metallogeny of mainland Southeast Asia– a review and contribution. Gondwana Res 26:5–30

Zhang M, O'Reilly SY, Chen D (1999) Location of Pacific and Indian mid-ocean ridge-type mantle in two time slices: evidence from Pb,

Sr and Nd isotopes for Cenozoic Australian basalts. Geology 27:39–42

Zhang J-J, Zheng Y-F, Zhao Z-F (2009) Geochemical evidence for interaction between oceanic crust and lithospheric mantle in the origin of Cenozoic continental basalts in east-central China. Lithos 110:305–326

Zhao D, Piranjo F, Dobretsov I, Lui L (2010) Mantle structure and dynamics under East Russia and adjacent regions. Russ Geol Geophys 51:925–938

Zheng J, Sun M, Zhou M-F, Robinson P (2005a) Trace elemental and PGE geochemical constraints of Mesozoic and Cenozoic peridotitic xenoliths on lithospheric evolution of the North China Craton. Geochem Cosmochim Acta 69:3401–3418

Zheng Y-F, Wu Y-B, Zhao Z-F, Zhang S-B, Xu P, Wu F-Y (2005b) Metamorphic effect on zircon Lu-Hf and U-Pb systems in ultrahigh pressure eclogite-facies metagranite and metabasite. Earth Planet Sci Lett 240:378–400

Zou H, Zindler A, Xu X, Qi Q (2000) Major, trace element and Nd, Sr and Pb isotope studies of Cenozoic basalts in SE China: mantle sources, regional variations, and tectonic significance. Chem Geol 171:33–47